Quantum Methodologies for the simulation of molecular hydrogen: from dimers to linear chains

by

Adam Marr

A thesis

presented to the University of Waterloo

in fulfillment of the

thesis requirement for the degree of

Master of Science

in

Chemistry

Waterloo, Ontario, Canada, 2020

© Adam Marr 2020

Author's Declaration

This thesis consists of material all of which I authored or co-authored: see Statement of Contributions included in the thesis. This is a true copy of the thesis, including any required final revisions, as accepted by my examiners.

I understand that my thesis may be made electronically available to the public.

Statement of Contributions

This thesis consists of previous work that has been submitted and accepted for publication:

(1) Marr, A.; Halverson, T.; Tripp, A.; Roy, P.-N. J. Phys. Chem. A 2020, 124, 6877–6888. Copyright 2020 American Chemical Society.

In Chapter 1, we use some of the introduction from the paper; Chapter 2 consists of theory from the article; and Chapter 3 consists of the bulk of the article.

As lead author of this publication, I was responsible for preparing and writing the manuscript for this article.

Abstract

Hydrogen has long been considered an ideal model system for a variety of molecular configurations, given its chemical simplicity and ubiquitous nature in the world. However, the weak van der Waals forces that exist between hydrogen molecules have often been challenging to model, with work in developing a thorough analytical and numerical potential energy surface dating back decades. In this thesis, we consider a theoretical approach to hydrogen-based systems. We draw on well known properties of spherical harmonics to produce vibrational Raman and Infrared results, with good agreement to prior experimental work and for the prediction of results for isotopologues involving deuterium and tritium. As part of this analysis, both spin isomers (para and ortho) are considered; a full range of nuclear spin considerations are discussed as a means of helping to explore spectroscopic intensities. We consider efficient diagonalization techniques and basis reduction tools, in conjunction with the general theme of symmetrization. This model is also extended to an adiabatic setup, where a more 'primitive' basis is considered; in this configuration, the rotors are assumed to be decoupled from one another without end-over-end rotation of the dimer and are fixed in space. By analyzing the various states at different intermolecular distances, we are able to explore the suitability of this model in comparison to the full coupled results. We then extend these findings to chains of hydrogen molecules; here, we explore both an exact diagonalization technique as well as a singular value decomposition and one-body operator method for use with the density matrix renormalization group. Ultimately, this work will help lay a foundation for other arrangements of hydrogen (e.g. clusters, solid hydrogen) and similar homonuclear diatomic molecules, such as nitrogen or oxygen.

Acknowledgements

I would like to thank my supervisor Professor Pierre-Nicholas Roy for all of his support and encouragement during the course of my time in his research group; his constant guidance and advice were invaluable both in writing this thesis and helping me succeed in this program. Thank you as well to the other members of my supervisory committee (Professors Marcel Nooijen and Scott Hopkins) for their assistance. I would also like to thank in particular Dr. Thomas Halverson and Austin Tripp for the many discussions, code, and notes/equations used for developing an analytical solution for the rotating hydrogen dimer; Dmitri Iouchtchenko for advice on implementing the many-rotors model and for his notes/equations deriving the DMRG approach; Fiorella Villanueva Heldmaier for providing her valuable support and comments on this thesis; and Alexander Ibrahim for help in debugging (again and again). Special thanks to my mother Susan Marr for providing constant support and helpful grammatical edits on this thesis. Much appreciation as well to current and former members of the Theoretical Chemistry group (including Matthew Schmidt, Xichen Lou, Tapas Sahoo, Kevin Bishop, Spencer Yim, and Neil Raymond) for fostering a great environment to work and grow in as a graduate student.

Dedication

To my family-I love you now and forever.

Table of Contents

List of Figures

List of Tables

List of Abbreviations

DMRG   Density matrix renormalization group

EQQ   Electric quadrupole-quadrupole

FCC   Face-centred cubic

HCP   Hexagonal closed-packed

IR   Infrared

Itensor   Intelligent tensor

LM   Largest magnitude

MPO   Matrix product operator

MPS   Matrix product states

pH_2 Para hydrogen

PES   Potential energy surface

oH_2 Ortho hydrogen

SA   Smallest algebraic

SVD   Singular value decomposition

Chapter 1

Introduction

As the most common element in the universe, hydrogen is an essential component of numerous molecules. In particular, molecular hydrogen (H_2) has a wide range of applications, from its use as a clean source of fuel[1] to its presence in many chemical reactions.[2] The ability to store hydrogen molecules for later use has also prompted significant research; ongoing work focuses on structures such as carbon nanotubes[3] or water-based clathrates[4] as potential mediums for clusters or chains of molecules. As part of this research, it is essential to have an understanding of how hydrogen molecules interact with each other to produce forms as diverse as dimers, chains, and solid configurations. Despite the simplicity of hydrogen atoms and molecules, substantial work has been devoted to creating increasingly complex intermolecular potential energy surfaces. As will be explored throughout this thesis, these efforts have become very successful in reproducing and helping to predict experimental spectroscopic results.

1.1 Ortho and Para Hydrogen: Nuclear Spin Statistics

As described by Van Kranendonk,[5] the number of protons and neutrons within an atom's nucleus are responsible for determining a parameter known as nuclear spin. If a nucleus has some spin I, there will be a total of $2I + 1$ degenerate nuclear spin states ($|Im\rangle$). However, identical atoms can undergo exchange of their nuclei, producing a new quantity known as $\boldsymbol{I_T}$ that represents the total spin. In general, I_T spans $\{|I_1 - I_2| \ldots (I_1 + I_2)\}$ since $\boldsymbol{I_T} = \boldsymbol{I_1} + \boldsymbol{I_2}$. For the special case of identical molecules, $I_1 = I_2 = I$, the possible values for $\boldsymbol{I_T}$ are $0, \ldots, 2I - 1, 2I$. To determine the combined coupled spin states $|I_T m_T\rangle$, we can rewrite the equation in terms of a tensor product of the two individual spin states, where we add a Clebsch-Gordan coefficient for each product and apply a summation:[6]

$$|I_T m_T\rangle = \sum_{m_1, m_2} C_{Im_1 Im_2}^{I_T m_T} |Im_1\rangle_1 |Im_2\rangle_2 \tag{1.1}$$

The nuclei of particles are characterized as bosons and fermions if they have integer or non-integer spin, respectively. The primary distinction between these two categories is the mathematical result that occurs upon exchange of two identical particles. In particular, in terms of their total wavefunctions, fermions are antisymmetric upon exchange, whereas bosons are symmetric upon exchange. These total wavefunctions can be thought of as a product of each individual component wavefunction: $\Psi_T = \Psi_{el} \Psi_{vib} \Psi_{rot} \Psi_{ns}$. For ^{1}H, $I = \frac{1}{2}$, indicating that the nucleus is a fermion and requiring that the total nuclear wavefunction be antisymmetric upon exchange of the two hydrogen nuclei. This property takes into account the swapping of the internuclear separation variable r with the term $-r$ that dictates the

symmetry of the orbital component of the wavefunction, such that it is paired properly with either a symmetric or antisymmetric nuclear spin wavefunction.[5] Note that the ground electronic state for H_2 is $^1\Sigma_g^+$, which is symmetric upon exchange. The vibrational ground state is also symmetric, since the wavefunction is invariant of the sign change of r. By contrast, the parity of the spherical harmonics $(-1)^j$ produces symmetric rotational wavefunctions for even j values and antisymmetric rotational wavefunctions for odd j values (for a $180°$ rotation). Therefore, for H_2:

$$\Psi_{tot}(AS) = \Psi_{el}(S) * \Psi_{vib}(S) * \begin{cases} \Psi_{rot,even}(S) * \Psi_{ns}(AS) \\ \\ \Psi_{rot,odd}(AS) * \Psi_{ns}(S) \end{cases} \tag{1.2}$$

Here, we see that the sign of Ψ_{ns} is determined using the known properties of Clebsch-Gordan coefficients that allow us to determine the symmetry of the spin function. In particular, exchanging particles 1 and 2 results in an identical result with the addition of a phase factor:[5]

$$\hat{P}_{12}\left|I_T m_T\right\rangle = \sum_{m_1,m_2} (-1)^{I+I-I_T} C_{Im_2 Im_1}^{I_T m_T} \left|Im_2\right\rangle_2 \left|Im_1\right\rangle_1$$
$$= (-1)^{2I-I_T} \left|I_T m_T\right\rangle \tag{1.3}$$

Based on the above equation, for non-integer spin, when $2I - I_T$ is odd, Ψ_{ns} is antisymmetric and produces $(2I+1)I$ states (singlet, H_2, para, $I_T = 0$). If $2I - I_T$ is even, Ψ_{ns} is symmetric and produces $(2I+1)(I+1)$ states (triplet, H_2, ortho, $I_T = 1$).[5] Ortho hydrogen is restricted to odd rotational levels, while para hydrogen is limited to even rotational levels for ground and excited vibrational states. This ratio between ortho and para hydrogen defines the upper

boundary of ortho hydrogen at high temperatures with a fixed 3:1 equilibrium between the two forms. However, as the temperature decreases, the equilibrium shifts in favour of para hydrogen, approaching a pure form (Figure 1.1) as a consequence of Boltzmann statistics. Note that all plots shown throughout this work were created using the Matplotlib software package.[7]
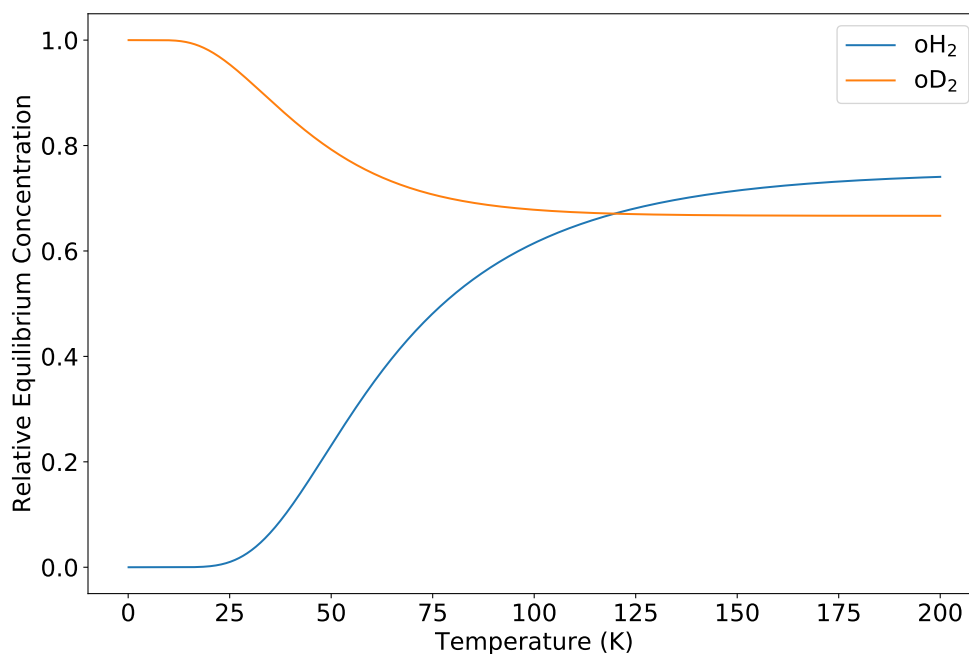
Figure 1.1: Relative ortho equilibrium concentrations for compounds containing H_2 or D_2 at different temperatures. At high temperatures, ortho H_2 and D_2 dominate at ratios of 3:1 and 2:1, respectively, in comparison to the corresponding para spin isomer. By contrast, at low temperatures, the mixtures are nearly pure para H_2 and ortho D_2.[5]

1.2 Hydrogen Dimers

The weakly-bound van der Waals dimer $(H_2)_2$ has been a source of fascination and study for decades. It was first discovered by Watanabe and Welsh in 1964,[8] who identified the dimer

4
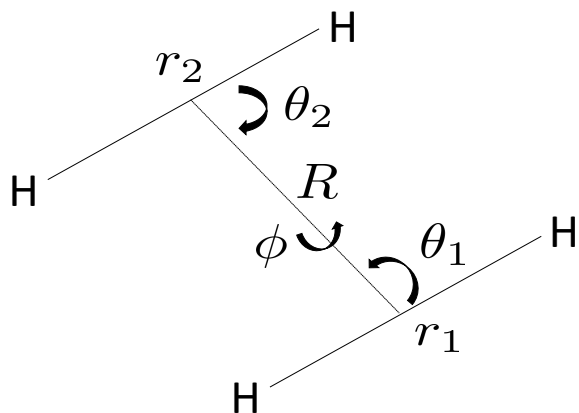
Figure 1.2: 6D Body-fixed representation of the $(H_2)_2$ dimer, consisting of three radial (r_1, r_2, R) and three angular coordinates $(\theta_1, \theta_2, \phi)$.

using infrared (IR) spectroscopy on samples of pure para hydrogen (pH_2) and normal gaseous H_2 containing hydrogen's other spin isomer, ortho hydrogen (oH_2). Further investigation by McKellar and coworkers[9–12] verified the presence of $(H_2)_2$, with additional rovibrational lines. Theoretical studies have sought to complement these experimental results, focusing on producing an accurate potential energy surface (PES) that allows for the prediction of spectral lines.[13–20] In 2008, Hinde[19] introduced a six dimensional setup, consisting of three radial (r_1, r_2, R) and three angular (θ_1 , θ_2 , ϕ) components (Figure 1.2). As part of his investigation, Hinde successfully confirmed several rovibrational lines described by McKellar for pH_2-pH_2 dimers using IR spectroscopy. However, given that hydrogen molecules lack a permanent dipole moment and only possess a weak quadrupole, Raman spectroscopy is a more viable alternative for the detection of clusters. Production of small ($N = 2 - 8$) para hydrogen clusters has been shown to be possible through the use of cryogenic free jets.[21] Hinde's model accurately predicted a Raman shift of -0.4 cm^{-1} for the dimer, relative to the Q(0) monomer spectral line. Over the past few years, para hydrogen clusters have been explored

in more depth. Motivated by Hinde's results, an adiabatic Hindered (1D) rotor potential was constructed from the 6D model,[22,23] in tangent with related studies involving pH_2-CO_2,[24] pH_2-H_2O,[25] pH_2-N_2O,[26] and pH_2-CH_3F[27] complexes. While other approaches have relied on adiabatic corrections to a Born-Oppenheimer model involving nuclear and electronic coordinates of the hydrogen dimer,[28] the adiabatic 1D rotor model focuses on separating the fast motion along the dimer coordinates (r_1, r_2, θ_1 , θ_2 , ϕ) from the slow motion along the coordinate R. Given the difficulty in producing and isolating ortho hydrogen-containing dimers at low temperatures, little experimental work has been performed for ortho-para and ortho-ortho hydrogen dimers. A recent theoretical paper investigated the applicability of this potential in solid para hydrogen, using a path integral method.[29] However, cryogenic free jets have also been used to produce mixed hydrogen clusters.[30] This setup allowed for the identification of oH_2-pH_2 and oH_2-oH_2 hydrogen dimers using Raman spectroscopy, with observed shifts of approximately -0.3 cm^{-1} from the Q(0) and Q(1) lines and -0.4 cm^{-1} from the Q(1) line, respectively.

1.3 Solid Hydrogen

Research on solid hydrogen provides an additional opportunity for observing fascinating characteristics of both ortho and para hydrogen. In particular, there has been significant interest in impurities within solid hydrogen that affect the physical properties of the structure. At equilibrium, experimental evidence has suggested that solid hydrogen forms in a hexagonal close-packed (hcp) structure preferentially over a face-centred cubic (fcc) structure;[5] recent theoretical work has helped confirm this idea.[29,31] At atmospheric pressure, solid hy-

drogen forms only at low temperatures (<14.01 K),[32] producing structures that are nearly entirely composed of para hydrogen. These structures can lead to a number of interesting spectroscopic results. In general, no Q(0) infrared spectrum peak can be detected since the symmetry of the complex leads to a net induced dipole of zero,[33] while the Q(0) quadrupole transition is also forbidden.[34] However, if a "dopant" or "impurity" is introduced within the structure, the net induced dipole is no longer zero and IR peaks can be observed.[35] A number of different molecules can be used as possible impurities, with various effects on the resulting IR specta to produce a shifted, narrowed Q(0) line (around 4149-4152 cm^{-1} in solid hydrogen).[33,35] In particular, increasing the concentration of ortho hydrogen in the sample introduces impurities in the clusters and produces an IR peak.[5,36] Noble gases (e.g. Ar, Kr, Xe) are also able to produce distinguishable Q(0) peaks, with downward shifts in energy due to the formation of X-H_2 complexes, with the intensity of the IR signal varying depending on the strength of the interaction between the hydrogen molecule and introduced impurity.[33]

1.4   Structure of Thesis

This thesis is divided into four additional technical and application chapters, and a conclusion. Chapter 2 outlines a theoretical framework for the exact ('full') and adiabatic hydrogen dimer models; these models, with comparisons to experimental data, are described in Chapters 3 and 4, respectively. Chapter 5 extends this model using exact diagonalization and the density matrix renormalization group (DMRG), using a mix of analytical one body operators as well as a singular value decomposition (SVD) method.

Chapter 2

Theoretical Framework

In this chapter, we present a summary of the coupling mechanisms for various basis sets, including the close-coupled approach developed previously,[37–40] which is applied for the hydrogen dimer system in Chapter 3. These equations are formed based on the scattering approach of two rotors first introduced by Klar.[37] We also consider the effects of varying levels of coupling on the labeling of eigenvalues. Before considering the exact nature of our potential energy matrix elements, let us consider the components of the chosen basis sets. For a dimer system, the two hydrogen molecules have angular momentum quantum numbers j_1 and j_2, with projections m_1 and m_2, respectively. In the space-fixed frame, the dimer itself has some separate quantum number L_{end} with projection $M_{L_{end}}$ which defines the end-over-end rotation of the dimer as a whole. When defining our basis set, we can couple various parts of our basis sets together; this property allows us to sum over different m projections, reducing the ultimate size of our basis set. The addition or lack of coupling produces different potential energy matrix elements, since we are making use of different representations of the chosen basis set. However, in certain cases, we can also exclude components of the basis set from consideration; in particular, the 'partial' and 'primitive' coupling approaches described

below neglect the end-over-end rotation quantum number L_{end} in contrast to its inclusion in the 'Full' close-coupled approach.

2.1   Full close-coupled approach

In this setup, we assume that $\boldsymbol{j_1} + \boldsymbol{j_2} = \boldsymbol{j_{12}}$ and $\boldsymbol{L_{end}} + \boldsymbol{j_{12}} = \boldsymbol{J}$. Of these quantum numbers, only J is conserved (i.e. $[\hat{H}, \boldsymbol{J}]=0$). This property ensures that J is both diagonal and that its corresponding projection M plays no role in the value of the obtained potential (i.e. it is rotationally invariant).[37] Note that our angular wavefunction is given as a tripolar spherical harmonic:[19,39]

$$I_{J,M,j_1,j_2,j_{12},L_{end}}(\hat{\boldsymbol{r}}_1, \hat{\boldsymbol{r}}_2, \hat{\boldsymbol{R}}) = \sum_{m_1 m_2 m_{12} M_{L_{end}}} C^{j_{12}m_{12}}_{j_1 m_1 j_2 m_2} C^{JM}_{j_{12}m_{12}L_{end}M_{L_{end}}}$$

$$\times Y_{j_1,m_1}(\hat{\boldsymbol{r}}_1) Y_{j_2,m_2}(\hat{\boldsymbol{r}}_2) Y_{L_{end},M_{L_{end}}}(\hat{\boldsymbol{R}}) \qquad (2.1)$$

In the above equation, the notation $C^{j_3 m_3}_{j_1 m_1 j_2 m_2}$ is used as a standard representation for Clebsch-Gordan coefficients. Our potential operator $\hat{V}_{12}$ is divided into two different parts: a radial operator $\hat{A}_{l_1,l_2,L}$ and an angular operator $\hat{G}_{l_1,l_2,L}$. The angular operator is a zero rank tensor, composed of the scalar product of a bipolar spherical harmonic and another spherical harmonic.[37] Note that the chosen expansion for l_1, l_2, L differs for a particular system depending on the importance of each term, e.g. for the hydrogen dimer, the following expansions are the most important: $(l_1, l_2, L) = (000, 022, 202, 224)$. Throughout this chapter, we focus primarily on an exact, analytical expression for the $\hat{G}_{l_1,l_2,L}$ operator. For the radial portion of the potential, we use a simple expression of $A_{l_1,l_2,L}(R)$. In Chapter 3, when

9

we make use of Hinde's[19] 6D potential, we describe vibrationally averaged values for the potential as $\langle \nu_1 j_1 \nu_2 j_2 | \hat{A}_{l_1,l_2,L} | \nu_1' j_1' \nu_2' j_2' \rangle$. Notably, these values take into account a $(4\pi)^{-3/2}$ term that is produced during the exact integration of spherical harmonics in the analytical expression. This property allows for a simplification of the explicit $\hat{G}_{l_1,l_2,L}$ terms and matrix elements. For instance, in a body-fixed frame, these terms are defined as:[16]

$$\hat{G}_{000}(\theta_1, \theta_2, \phi) = 1 \tag{2.2}$$

$$\hat{G}_{022}(\theta_1, \theta_2, \phi) = \frac{5}{2}(3\cos^2(\theta_2) - 1) \tag{2.3}$$

$$\hat{G}_{202}(\theta_1, \theta_2, \phi) = \frac{5}{2}(3\cos^2(\theta_1) - 1) \tag{2.4}$$

$$\hat{G}_{224}(\theta_1, \theta_2, \phi) = \frac{45}{4\sqrt{70}}[2(3\cos^2(\theta_1) - 1)(3\cos^2(\theta_2) - 1)$$

$$- 16\sin(\theta_1)\cos(\theta_1)\sin(\theta_2)\cos(\theta_2)\cos(\phi)$$

$$+ \sin^2(\theta_1)\sin^2(\theta_2)\cos(2\phi)] \tag{2.5}$$

In our space-fixed frame, we instead define these terms as the following, beginning without any initial $(4\pi)^{-3/2}$ normalization:[6,37]

$$\hat{G}_{l_1,l_2,L}(\hat{\boldsymbol{r}}_1, \hat{\boldsymbol{r}}_2, \hat{\boldsymbol{R}}) = \{Y_{l_1}(\hat{\boldsymbol{r}}_1) \otimes Y_{l_2}(\hat{\boldsymbol{r}}_2)\}_{Lm_L} \cdot Y_L(\hat{\boldsymbol{R}}) \tag{2.6}$$

$$= \sum_{m_{l_1} m_{l_2} m_L} C^{Lm_L}_{l_1 m_{l_1} l_2 m_{l_2}} Y_{l_1,m_{l_1}}(\hat{\boldsymbol{r}}_1) Y_{l_2,m_{l_2}}(\hat{\boldsymbol{r}}_2) Y_{L,m_L}(\hat{\boldsymbol{R}})^* \tag{2.7}$$

$$= Y_L(\hat{\boldsymbol{R}}) \cdot Y_L^{l_1 l_2}(\hat{\boldsymbol{r}}_1, \hat{\boldsymbol{r}}_2) \tag{2.8}$$

We can express this fully in matrix element form with the basis $|j_1 j_2 j_{12} L_{end} JM\rangle$:[37]

$$\langle j_1 j_2 j_{12} L_{end} JM| \hat{V}_{12} |j_1' j_2' j_{12}' L_{end}' J'M'\rangle = \sum_{l_1 l_2 L} A_{l_1 l_2 L}(R)$$

$$\times \langle j_1 j_2 j_{12} L_{end} J|| \boldsymbol{Y_L} \cdot \boldsymbol{Y_L^{l_1 l_2}} ||j_1' j_2' j_{12}' L_{end}' J'\rangle \quad (2.9)$$

Using Eq. 5.13 from Brink and Satchler,[41] we can write the following expression. Note that $[x] = 2x + 1$ and that W denotes a Racah coefficient:

$$\langle j_1 j_2 j_{12} L_{end} J|| \boldsymbol{Y_L} \cdot \boldsymbol{Y_L^{l_1 l_2}} ||j_1' j_2' j_{12}' L_{end}' J'\rangle = (-1)^{J - L_{end} - j_{12}'} W(L_{end} L_{end}' j_{12} j_{12}'; LJ)$$

$$\times \langle L_{end}|| \boldsymbol{Y_L} ||L_{end}'\rangle$$

$$\times \langle j_1 j_2 j_{12}|| \boldsymbol{Y_L^{l_1, l_2}} ||j_1' j_2' j_{12}'\rangle \, \delta_{J,J'} \delta_{M,M'} \quad (2.10)$$

Where (using Eq. 5.12 from Brink and Satchler):

$$\langle L_{end}|| \boldsymbol{Y_L} ||L_{end}'\rangle = \left(\frac{[L_{end}'][L]}{4\pi} \right)^{1/2} C_{L_{end}' 0 L 0}^{L_{end} 0} \quad (2.11)$$

In the above equation, we follow the convention from Varshalovich[6] (see Eq. 13.2.8(105) versus Eq. 4.17 from Brink and Satchler) for the form of the reduced matrix elements, such that our reduced matrix element term is $[L_{end}]^{1/2}$ greater than the equivalent term given by Brink and Satchler, which has an additional factor of $[L_{end}]^{-1/2}$ in Eq. 2.11. We continue this convention below for the expansion of the reduced matrix elements below, relying on a modified Eq. 5.12 from Brink and Satchler (e.g. we have included the $[j_{12}]^{1/2}$ factor in this equation as opposed to the previous equation).

$$\langle j_1 j_2 j_{12} || \boldsymbol{Y_L^{l_1,l_2}} || j_1' j_2' j_{12}' \rangle = ([j_{12}][j_{12}'][L])^{1/2} \begin{Bmatrix} j_{12} & j_{12}' & L \\ j_1 & j_1' & l_1 \\ j_2 & j_2' & l_2 \end{Bmatrix}$$

$$\times \langle j_1 || \boldsymbol{Y_{l_1}} || j_1' \rangle \langle j_2 || \boldsymbol{Y_{l_2}} || j_2' \rangle \qquad (2.12)$$

$$= ([j_{12}][j_{12}'][L])^{1/2} \begin{Bmatrix} j_{12} & j_{12}' & L \\ j_1 & j_1' & l_1 \\ j_2 & j_2' & l_2 \end{Bmatrix}$$

$$\times \left(\frac{[j_1'][l_1]}{4\pi} \right)^{1/2} C_{j_1' 0 l_1}^{j_1 0} \left(\frac{[j_2'][l_2]}{4\pi} \right)^{1/2} C_{j_2' 0 l_2}^{j_2 0} \qquad (2.13)$$

The final form given by Green is presented slightly different, using Wigner-3j and Wigner-6j symbols instead of Clebsch-Gordan and Racah coefficients, respectively. First, let us consider Eq. 8.1.2(12) from Varshalovich to convert the Clebsch-Gordan coefficients to Wigner-3j symbols:

$$C^{L_{end}0}_{L'_{end}0L0} = (-1)^{L'_{end}-L}[L_{end}]^{1/2} \begin{pmatrix} L'_{end} & L & L_{end} \\ 0 & 0 & 0 \end{pmatrix} \tag{2.14}$$

$$C^{j_10}_{j'_10l_10} = (-1)^{j'_1-l_1}[j_1]^{1/2} \begin{pmatrix} j'_1 & l_1 & j_1 \\ 0 & 0 & 0 \end{pmatrix} \tag{2.15}$$

$$C^{j_20}_{j'_20l_20} = (-1)^{j'_2-l_2}[j_2]^{1/2} \begin{pmatrix} j'_2 & l_2 & j_2 \\ 0 & 0 & 0 \end{pmatrix} \tag{2.16}$$

Now, we use Eqs. 9.4.3(5) and 9.1.2(11) from Varshalovich to convert Racah coefficients to Wigner-6j symbols:

$$W(L_{end}L'_{end}j_{12}j'_{12}; LJ) = W(L'_{end}L_{end}j'_{12}j_{12}; LJ) \tag{2.17}$$

$$= (-1)^{L'_{end}+L_{end}+j_{12}+j'_{12}} \begin{Bmatrix} L'_{end} & L_{end} & L \\ j_{12} & j'_{12} & J \end{Bmatrix} \tag{2.18}$$

For each of the above Wigner-3j symbols, the following relationship is true (see Eq. 8.4.2(5) of Varshalovich):

$$\begin{pmatrix} j_a & j_b & j_c \\ 0 & 0 & 0 \end{pmatrix} = (-1)^{j_a+j_b+j_c} \begin{pmatrix} j_b & j_a & j_c \\ 0 & 0 & 0 \end{pmatrix} \tag{2.19}$$

$(j_a + j_b + j_c)$ must be even for all of these results or else the resulting term is equal to 0 (see Eq. 8.5.2(32)) and the phase can be discarded for these terms. If we make this conversion and sum up all of the others parities, we are left with the following result:

$$(J - L_{end} - j'_{12}) + (L'_{end} - L) + (j'_1 - l_1) + (j'_2 - l_2) + (L'_{end} + L_{end} + j_{12} + j'_{12})$$

$$= J + 2L'_{end} + j'_1 + j'_2 + j_{12} - l_1 - l_2 - L \quad (2.20)$$

Since L'_{end} is an integer, $2L'_{end}$ is an even integer, and can be discounted. Similarly, $-(l_1 + l_2 + L)$ is also even. Our final expression for the phase is therefore $(-1)^{J+j'_1+j'_2+j_{12}}$. In addition, from Eq. 10.4.1(6) from Varshalovich:

$$\begin{Bmatrix} j_{12} & j'_{12} & L \\ j_1 & j'_1 & l_1 \\ j_2 & j'_2 & l_2 \end{Bmatrix} = \begin{Bmatrix} j'_{12} & j'_2 & j'_1 \\ j_{12} & j_2 & j_1 \\ L & l_2 & l_1 \end{Bmatrix} \quad (2.21)$$

A slightly different final phase can be derived instead: $(-1)^{J+j_1+j_2+j'_{12}}$, which is equivalent to the form from above and makes use of the symmetry and phase change properties associated with Wigner 3-j and 6-j symbols, as well as some prior conventions used in deriving this result. We therefore obtain the final expression for the potential energy matrix elements written in the same final form as Green,[39] where $|\lambda\rangle = |j_1 j_2 j_{12} L_{end} J\rangle$:

$$\langle \lambda | \hat{V}_{12} | \lambda' \rangle = \sum_{l_1 l_2 L} A_{l_1 l_2 L}(R) (4\pi)^{-3/2} (-1)^{J+j_1+j_2+j'_{12}}$$

$$\times \left([L]^2 [l_1][l_2][j_1][j_2][j_{12}][L_{end}][j'_1][j'_2][j'_{12}][L'_{end}]\right)^{1/2}$$

14

$$\times \begin{pmatrix} L & L'_{end} & L_{end} \\ 0 & 0 & 0 \end{pmatrix} \begin{pmatrix} l_1 & j'_1 & j_1 \\ 0 & 0 & 0 \end{pmatrix} \begin{pmatrix} l_2 & j'_2 & j_2 \\ 0 & 0 & 0 \end{pmatrix}$$

$$\times \begin{Bmatrix} L'_{end} & L_{end} & L \\ j_{12} & j'_{12} & J \end{Bmatrix} \begin{Bmatrix} j'_{12} & j'_2 & j'_1 \\ j_{12} & j_2 & j_1 \\ L & l_2 & l_1 \end{Bmatrix} \delta_{J,J'} \delta_{M,M'} \tag{2.22}$$

2.2 'Partial' close-coupled approach

Suppose we remove end-over-end rotation, i.e. the quantum number L_{end}, and consequently, the total angular momentum J. However, j_{12} is not a conserved quantity and is not rotationally invariant (i.e. $[\hat{H}, \boldsymbol{j_{12}}] \neq 0$). In other words, our new basis set is $|j_1 j_2 j_{12} m_{12}\rangle$, where our angular wavefunction is a bipolar spherical harmonic:

$$I_{j_1,j_2,j_{12},m_{12}}(\hat{\boldsymbol{r}}_{\boldsymbol{1}}, \hat{\boldsymbol{r}}_{\boldsymbol{2}}) = \sum_{m_1 m_2} C^{j_{12} m_{12}}_{j_1 m_1 j_2 m_2} Y_{j_1,m_1}(\hat{\boldsymbol{r}}_{\boldsymbol{1}}) Y_{j_2,m_2}(\hat{\boldsymbol{r}}_{\boldsymbol{2}}) \tag{2.23}$$

Our angular operator is the same as before; however, the dimer is now fixed at a specific angle. Nevertheless, this should not have a particular effect on the PES, since it is rotationally invariant of the direction that is set for the space-fixed axis.[39] We therefore first consider a dimer fixed along the z-axis (with $\hat{\boldsymbol{R}} = (0,0)$). This form is convenient since $Y_{L,M_L}(0,0) = [\frac{2L+1}{4\pi}]^{1/2} \delta_{M_L 0}$. Our potential operator parameterized at these coordinates take the form:

$$\hat{G}_{l_1,l_2,L}(\hat{\boldsymbol{r}}_{\boldsymbol{1}}, \hat{\boldsymbol{r}}_{\boldsymbol{2}}; \hat{\boldsymbol{R}} = (\boldsymbol{0},\boldsymbol{0})) = \{\hat{Y}_{l_1,m_1}(\hat{\boldsymbol{r}}_{\boldsymbol{1}}) \otimes \hat{Y}_{l_2,m_2}(\hat{\boldsymbol{r}}_{\boldsymbol{2}})\}_{L0} \tag{2.24}$$

$$= \sqrt{\frac{2L+1}{4\pi}} \sum_m C^{L0}_{l_1 m l_2 -m} \hat{Y}_{l_1,m}(\hat{\boldsymbol{r}_1}) \hat{Y}_{l_2,-m}(\hat{\boldsymbol{r}_2}) \qquad (2.25)$$

Where, using the Wigner-Eckart Theorem, we arrive at a similar equation derived previously.[42–44] Notably, this equation is identical to the matrix elements that can be obtained for a rotating, body-fixed representation of the potential matrix element, with one important distinction: our dimer is not rotating and is still in the space-fixed frame. Consequently, any kinetic or angular momentum operator that we add to this equation would still be associated with the space-fixed frame as well. Therefore, fixed along this coordinate:

$$\langle j_1 j_2 j_{12} m_{12} | \hat{V}_{fixed} | j_1' j_2' j_{12}' m_{12}' \rangle = \sum_{l_1 l_2 L} A_{l_1 l_2 L}(R) \sqrt{\frac{2L+1}{4\pi}} C^{j_{12} m_{12}}_{j_{12}' m_{12}' L0} \frac{\langle j_1 j_2 j_{12} || \boldsymbol{Y}^{l_1,l_2}_{\boldsymbol{L}} || j_1' j_2' j_{12}' \rangle}{[j_{12}]^{1/2}}$$

$$(2.26)$$

$$= \sum_{l_1 l_2 L} A_{l_1 l_2 L}(R)(4\pi)^{-3/2}(-1)^{j_1'+j_2'+j_{12}'+m_{12}} \qquad (2.27)$$

$$\times ([L]^2 [l_1][l_2][j_1][j_2][j_{12}][j_1'][j_2'][j_{12}'])^{1/2}$$

$$\times \begin{pmatrix} l_1 & j_1' & j_1 \\ 0 & 0 & 0 \end{pmatrix} \begin{pmatrix} l_2 & j_2' & j_2 \\ 0 & 0 & 0 \end{pmatrix} \begin{pmatrix} j_{12}' & L & j_{12} \\ m_{12}' & 0 & -m_{12} \end{pmatrix} \begin{Bmatrix} j_{12}' & j_2' & j_1' \\ j_{12} & j_2 & j_1 \\ L & l_2 & l_1 \end{Bmatrix}$$

$$(2.28)$$

The above equation is similar to the form presented previously by Van Kranendonk[5] for a pair of interacting $j_1 = j_2 = 1$ molecules (refer to Eq. 7.18). His investigation only explores the ansiotropic contribution of the electric quadrupole-quadrupole (EQQ) interaction. Rewritten in our notation using the Wigner-Eckart theorem, this equation takes the following form (note the addition of the normalization factor $[j_{12}]^{1/2}$ based on our chosen convention for the definition of the reduced matrix element):

$$\langle j_1 j_2 j_{12} m_{12} | \hat{V}_{EQQ} | j_1' j_2' j_{12}' m_{12}' \rangle = C_{j_{12}' m_{12}' 40}^{j_{12} m_{12}} \frac{\langle j_1 j_2 j_{12} || \hat{V}_{EQQ} || j_1' j_2' j_{12}' \rangle}{[j_{12}]^{1/2}} \tag{2.29}$$

Where $\langle j_1 j_2 j_{12} || \hat{V}_{EQQ} || j_1' j_2' j_{12}' \rangle$ is the reduced matrix element for the EQQ model. The angular dependence of this interaction is identical to the expansion term $\hat{G}_{224}$ used in our model,[16] but does not include the anisotropy of the $\hat{G}_{022}$ and $\hat{G}_{202}$ expansions. However, in both cases, an additional restriction imposed here limits the basis size when the dimer lies along the collision axis, requiring $m_{12} = m_{12}'$ to produce non-zero values. Van Kranendonk represented this decoupling in a simple figure on page 202 (Figure 49),[5] with only the inclusion of a quadrupole force. If we now include all four terms, we can see that there is additional decoupling of states. This idea is presented in Figure 2.1, where we illustrate the effect of coupling on a minimum basis (i.e. $j_{1max} = j_{2max} = 1$). In particular, the initially isotropic potential consists of nine degenerate eigenstates, due to the symmetric nature of the isotropic $\hat{G}_{000}$ term. When the $\hat{G}_{224}$ operator is added, splitting begins to occur, such that for a fixed R, there exists some positive constant Γ_0, where the energy associated with each eigenstate $|j_{12} m_{12}\rangle$ is as follows:[5]

$(a)\, |20\rangle = 6\Gamma_0$

$(b,c)\,|2\pm2\rangle = \Gamma_0$

$(d)\,|10\rangle = 0,$

$(e)\,|00\rangle = 0,$

$(f,g)\,|1\pm1\rangle = 0,$

$(h,i)\,|2\pm1\rangle = -4\Gamma_0,$

In other words, the inclusion of this operator does not affect the diagonal nature of the resulting matrix. The addition of the $\hat{G}_{022}$ and $\hat{G}_{202}$ terms results in slight modifications to the potential energies. There are now, two degenerate lower $|1,\pm1\rangle = 0$ terms, one slightly higher $|00\rangle$ and one significantly higher $|10\rangle$ level. At different R distances, the relative energetic position of the $|1\pm1\rangle$ and $|00\rangle$ states can flip. However, the matrix is no longer completely diagonal, with small coupling between the $|20\rangle$ and $|00\rangle$ states. This is logical since only these terms share the same m_{12} states and $(-1)^{j_{12}}$ rotational symmetry. In summary, for our sample calculations using the labels a-g described in the text from above, we have three distinct cases at $R = 6.0\ a_0$. When only $\hat{G}_{000}$ is included:

$a = b = c = d = e = f = g = h = i$

In contrast, when $\hat{G}_{224}$ is also included:

$a > b = c > d = e = f = g > h = i$

Finally, when $\hat{G}_{022}$ and $\hat{G}_{202}$ are also included:

$a > b = c > d > e > f = g > h = i$
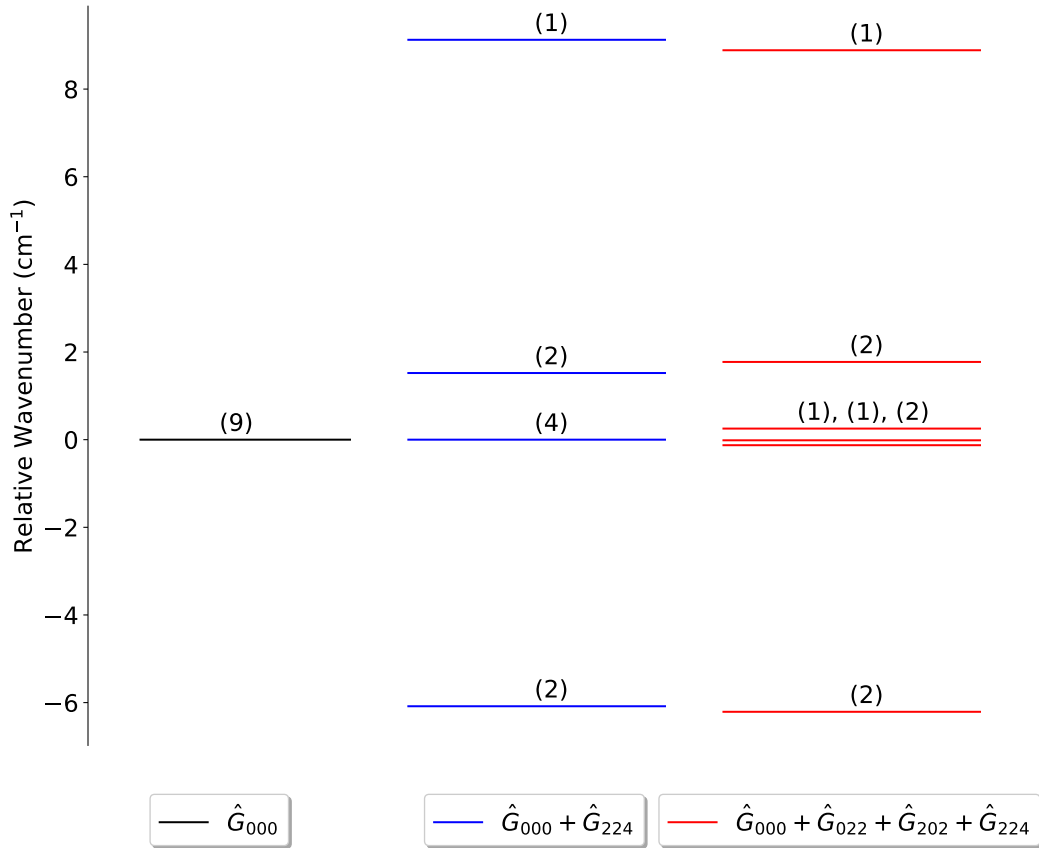
Figure 2.1: Effect of inclusion of various hydrogen angular expansion terms, fixed at a distance of 6.0 a_0 using Hinde's potential energy surface described in Chapter 3. Degeneracies of each state are included in brackets.

2.3 Primitive Basis

If we remove coupling between the two rotors (i.e. no j_{12}, m_{12}), we arrive at a final form derived previously that consists only of the 'primitive' basis functions (j_1, j_2, j_1', j_2' and the associated m values).[45] Note that this form is very similar to the equations presented in the previous section for the 'partial' coupled basis state; however, we no longer are able to neglect m_1 and m_2. While this results in a larger basis set for a dimer system, this formalism

is the foundation of a convenient basis state for rotor chains that we will explore in Chapter 5. For consistency, we present our Wigner-3j symbols using the corresponding order given in the text. Here, we again apply the Wigner-Eckart Theorem. We use the relationship $Y_{a,b}^* = (-1)^b Y_{a,-b}$ (Eq. 5.1.5(11)) in order to apply Eq. 5.9.1(5) for the integration of three spherical harmonics (refer to Varshalovich[6]), arriving at a form similar to that derived previously by Rabitz:[45]

$$\langle j_1 m_1 j_2 m_2 | \hat{V}_{fixed} | j_1' m_1' j_2' m_2' \rangle = \sum_{l_1 l_2 L} (-1)^{m_1+m_2} A_{l_1 l_2 L}(R)(4\pi)^{-3/2}$$

$$\times \sum_{m_{l_1}, m_{l_2}, M_L} C_{l_1 m_{l_1} l_2 m_{l_2}}^{L M_L} (4\pi)^{1/2} Y_{L M_L}(\hat{\boldsymbol{R}})^* ([l_1][l_2][j_1][j_2][j_1'][j_2'])^{1/2}$$

$$\times \begin{pmatrix} j_1 & l_1 & j_1' \\ -m_1 & m_{l_1} & m_1' \end{pmatrix} \begin{pmatrix} j_1 & l_1 & j_1' \\ 0 & 0 & 0 \end{pmatrix} \begin{pmatrix} j_2 & l_2 & j_2' \\ -m_2 & m_{l_2} & m_2' \end{pmatrix} \begin{pmatrix} j_2 & l_2 & j_2' \\ 0 & 0 & 0 \end{pmatrix}$$

$$(2.30)$$

In this equation, we can also apply a simplification when the space-fixed frame lies along the collision axis. As an additional benefit, the basis can be subdivided into non-coupling blocks, where $m_1 + m_2 = m_1' + m_2'$, based on the selection rules imposed by the Wigner 3j symbols and the shared values of m and $-m$. All of the matrix elements are real-valued due to the simple form of the spherical harmonic term:

$$\langle j_1 m_1 j_2 m_2 | \hat{V}_{fixed} | j_1' m_1' j_2' m_2' \rangle = \sum_{l_1 l_2 L} (-1)^{m_1+m_2} A_{l_1 l_2 L}(R)(4\pi)^{-3/2} \sum_m C_{l_1 m l_2 -m}^{L0}$$

$$\times ([L][l_1][l_2][j_1][j_2][j_1'][j_2'])^{1/2}$$

$$\times \begin{pmatrix} j_1 & l_1 & j_1' \\ -m_1 & m & m_1' \end{pmatrix} \begin{pmatrix} j_1 & l_1 & j_1' \\ 0 & 0 & 0 \end{pmatrix} \begin{pmatrix} j_2 & l_2 & j_2' \\ -m_2 & -m & m_2' \end{pmatrix} \begin{pmatrix} j_2 & l_2 & j_2' \\ 0 & 0 & 0 \end{pmatrix}$$

$$(2.31)$$

Ultimately, these approaches highlight an important idea: coupling changes the effective basis for our dimer. The circumstances in which each method can be employed may vary depending on the restrictions imposed on the system and/or the configuration (e.g. free rotating dimer pair vs. contained hydrogen chain, cluster, etc.). As we will see in Chapters 3 and 4, many of the quantum states exhibit degenerate energy values that can be predicted simply by looking at the analytical form of the potential.

2.4 Degeneracy of States

In considering the various matrix elements and basis sets throughout this chapter, one question comes to mind: what drives the energetic degeneracy that we see in these systems? In the 'full' close-coupled approach, the only degeneracy seen is associated with the projections of J (e.g. for J $= 1$, $M_J = (-1, 0, +1)$ states are all degenerate). As we break down the coupling, the relevant m values come out and do not always result in degeneracy. For the purely 'primitive' case, with non-coupling angular momentum fixed along the z-axis, we see that:

$$\begin{pmatrix} j_1 & l_1 & j_1' \\ -m_1 & m & m_1' \end{pmatrix} = (-1)^{j_1 + l_1 + j_1'} \begin{pmatrix} j_1 & l_1 & j_1' \\ m_1 & -m & -m_1' \end{pmatrix} \tag{2.32}$$

$$
\begin{pmatrix} j_2 & l_2 & j_2' \\ -m_2 & -m & m_2' \end{pmatrix} = (-1)^{j_2+l_2+j_2'} \begin{pmatrix} j_2 & l_2 & j_2' \\ m_2 & m & -m_2' \end{pmatrix} \tag{2.33}
$$

For our hydrogen-based systems, j_1 and j_1' must either be both odd or both even for a given spin isomer. The same is true for j_2 and j_2'. Note as well that l_1 and l_2 are always defined as either 0 or 2 for the potentials used in this investigation. Consequently, $j_1 + l_1 + j_1'$ and $j_2 + l_2 + j_2'$ are always even numbers and the phase will be equal to 1. As a result, there will exist an equivalent matrix element if the sign of the momentum projections is flipped, since the value of m extends from $-min\{l_1, l_2\}$ to $min\{l_1, l_2\}$. For instance, in the reduced basis set of $j_{1,max} = 1$ and $j_{2,max} = 0$ for an ortho-para hydrogen dimer, this property gives rise to two degenerate eigenvalues, composed of linear combinations of the $|j_1 m_1 j_2 m_2\rangle = |1100\rangle, |1\text{-}100\rangle$ eigenstates. As we will see in Chapter 4, however, there is a non-degenerate lower lying eigenstate composed entirely of $|1000\rangle$ when the dimer is fixed along the z-axis.

2.5 Symmetry

When exploring the dimer system, we made use of a symmetrized basis, described by Takayangi (1965)[46] for the close-coupled system. To ensure a linearly independent basis, we set $(\nu_1 < \nu_2)$ or $(\nu_1 = \nu_2$ and $j_1 \leq j_2)$ to generate the following potential energy matrix

elements:[1]

$$\langle\lambda|\,\hat{V}_{12}\,|\lambda'\rangle^{\pm} = [(1 + \delta_{\nu_1\nu_2}\delta_{j_1j_2})(1 + \delta_{\nu_1'\nu_2'}\delta_{j_1'j_2'})]^{-\frac{1}{2}} \Bigg(\langle\lambda|\,\hat{V}_{12}\,|\lambda'\rangle$$

$$\pm (-1)^{j_1+j_2-j_{12}+L_{end}} \langle\lambda_{sym}|\,\hat{V}_{12}\,|\lambda'\rangle \Bigg) \tag{2.34}$$

Where, $\lambda_{sym} = (\nu_2\nu_1j_2j_1j_{12}L_{end}J)$. For the primitive basis, the inclusion of m_1, m_2 and the removal of coupled variables J and L_{end} leads to a similar form for the symmetrized potential matrix elements. The reduced basis for this matrix takes the following form: $(\nu_1 < \nu_2)$ or $(\nu_1 = \nu_2$ and $j_1 \le j_2)$ or $(\nu_1 = \nu_2$ and $j_1 = j_2$ and $m_1 \le m_2)$:

$$\langle\nu_1j_1m_1\nu_2j_2m_2|\,\hat{V}_{12}\,|\nu_1'j_1'm_1'\nu_2'j_2'm_2'\rangle^{\pm} = [(1 + \delta_{\nu_1\nu_2}\delta_{j_1j_2}\delta_{m_1m_2})(1 + \delta_{\nu_1'\nu_2'}\delta_{j_1'j_2'}\delta_{m_1'm_2'})]^{-\frac{1}{2}}$$

$$\Bigg(\langle\nu_1j_1m_1\nu_2j_2m_2)|\,\hat{V}_{12}\,|\nu_1'j_1'm_1'\nu_2'j_2'm_2'\rangle$$

$$\pm \langle\nu_2j_2m_2\nu_1j_1m_1|\,\hat{V}_{12}\,|\nu_1'j_1'm_1'\nu_2'j_2'm_2'\rangle \Bigg) \tag{2.35}$$

Previous investigations[29] have instead relied on a projection operator approach, where the potential matrix is constructed from a full basis and symmetrized after the fact using matrix multiplication. In the symmetric ($\hat{S}$) and antisymmetric ($\hat{A}$) operators presented below, $\hat{I}$ is the identity operator and $\hat{P}_{12}$ is the permutation operator for ν_1, ν_2, j_1, j_2. For full coupling, the $(-1)^{j_1+j_2-j_{12}+L_{end}}$ phase factor is necessary to include the coupled rotational symmetry

---

[1]Some forms of potential energy matrix elements also make use of a symmetrized form of the $\hat{V}_{12}$ operator for identical particles (see, e.g. Alexander and DePristo[42]), so that only the l_1, l_2, L expansions $(0,0,0)$, $(0,2,2)$, and $(2,2,4)$ are required. While this ultimately involves one less potential energy term, the resulting symmetrized equations become more lengthy and do not appear to provide significant savings in time.

associated with the system into the equation:

$$\hat{S} = \frac{1}{2}(\hat{I} + (-1)^{j_1+j_2-j_{12}+L_{end}}\hat{P}_{12}) \tag{2.36}$$

$$\hat{A} = \frac{1}{2}(\hat{I} - (-1)^{j_1+j_2-j_{12}+L_{end}}\hat{P}_{12}) \tag{2.37}$$

With the matrix elements for the symmetrized and antisymmetrized matrices given by:

$$V_{ij_S} = \langle i| \hat{S}\hat{V}\hat{S} |j\rangle \tag{2.38}$$

$$V_{ij_A} = \langle i| \hat{A}\hat{V}\hat{A} |j\rangle \tag{2.39}$$

For the primitive basis, we arrive at a similar equation, but $\hat{P}_{12}$ is the permutation operator for $\nu_1, \nu_2, j_1, j_2, m_1, m_2$:

$$\hat{S} = \frac{1}{2}(\hat{I} + \hat{P}_{12}) \tag{2.40}$$

$$\hat{A} = \frac{1}{2}(\hat{I} - \hat{P}_{12}) \tag{2.41}$$

While this approach yields the same result, there are disadvantages associated with this method. In particular, there are no savings in basis size, as associated with the basis symmetrization technique. Furthermore, eigenvalues associated with antisymmetric and symmetric eigenfunctions default to a value of zero after symmetrization or antisymmetrization, respectively. This effect leads to a large number of degenerate eigenvalues; notably, ARPACK and other methods that rely on the Arnoldi method for eigenvalue problems can often struggle to find more than one eigenpair in the case of degenerate eigenvalues without further

24

modifications to algorithms.[47] More details surrounding the use of symmetry and matrix eigenvalue calculations are described in Chapter 3 and Appendix A, during our investigation of the full treatment of hydrogen dimers and isotopologues.

Chapter 3

Vibrational Raman Shifts of Spin Isomer Combinations of Hydrogen Dimers and Isotopologues

We extend[1] Hinde's model in reproducing the experimental Raman vibrational shifts of $(H_2)_2$ for all three dimer combinations. We also consider the analogous comparisons for observed and predicted $(D_2)_2$ and $(T_2)_2$ Raman results. For these full, exact diagonalization calculations, we make use of an analytical method developed previously.[39,40] Adopting this approach, we rely on exact solutions for the angular component of the potential that exploits the properties of analytical solutions containing Wigner 3-j, 6-j, and 9-j symbols. We provide considerations for the symmetry and nuclear spin statistics of the dimers and degeneracy of various binding energy states.

3.1 Theory

3.1.1 Exact Diagonalization

The dimer Hamiltonian is,

$$\hat{H} = \hat{T}_R + \hat{h}_1 + \hat{h}_2 + \hat{V}_{12} \tag{3.1}$$

where $\hat{T}_R$ is the kinetic energy operator associated with the relative motion of the monomers. Furthermore, $\hat{h}_1$ and $\hat{h}_2$ are the individual rovibrational monomer Hamiltonians. We choose as a basis the monomer eigenstates. They produce diagonal matrices such that each matrix element corresponds to energies calculated using Le Roy's[49] LEVEL code at different vibrational and rotational levels (ν and j). Specifically, this method relies on solving the radial Schrödinger equation and determining the energy eigenvalues and associated eigenfunctions for monomer hydrogen molecules. Finally, $\hat{V}_{12}$ is the potential energy operator for the two molecules. In line with Hinde[19] and Green's[39] notation and methods, we also define a nine-dimensional wavefunction derived previously:

$$\Psi(\boldsymbol{R}, \boldsymbol{r_1}, \boldsymbol{r_2}) = R^{-1} \sum_{\lambda} F_\lambda(R) I_{J,M,\gamma}(\hat{\boldsymbol{R}}, \hat{\boldsymbol{r}}_{\boldsymbol{1}}, \hat{\boldsymbol{r}}_{\boldsymbol{2}}) \psi_{\nu_1,j_1}(r_1) \psi_{\nu_2,j_2}(r_2) \tag{3.2}$$

where the vectors $\boldsymbol{r_1}$ and $\boldsymbol{r_2}$ describe the bond length, r_i, and orientation, (θ_i, ϕ_i), of each hydrogen molecule, while $\boldsymbol{R}$ is the Cartesian vector representing the difference between the centre of masses of the two monomers. Also, $\hat{\boldsymbol{r}}_{\boldsymbol{1}}(\theta_1, \phi_1) = \frac{\boldsymbol{r_1}}{r_1}$, $\hat{\boldsymbol{r}}_{\boldsymbol{2}}(\theta_2, \phi_2) = \frac{\boldsymbol{r_2}}{r_2}$, and $\hat{\boldsymbol{R}}(\theta_R, \phi_R) = \frac{\boldsymbol{R}}{R}$ are unit vectors parametrized by three sets of angular coordinates. As a shorthand, we represent sets of quantum numbers as $\gamma = (j_1 j_2 j_{12} L_{end})$ and $\lambda = (\nu_1 \nu_2 J M \gamma)$.

The angular basis function involves coupled angular momenta, such that vector sums are defined as $\boldsymbol{j_{12}} = \boldsymbol{j_1} + \boldsymbol{j_2}$ and $\boldsymbol{J} = \boldsymbol{j_{12}} + \boldsymbol{L_{end}}$. Eq. 3.2 consists of individual monomer wavefunctions ψ_{ν_1,j_1} (also obtained using the LEVEL code and orthonormalized), as well as a radial wavefunction, $F_\lambda(R)$, for the full dimer. The angular basis function $I_{J,M,\gamma}(\hat{\boldsymbol{R}}, \hat{\boldsymbol{r}_1}, \hat{\boldsymbol{r}_2})$ is defined as a tripolar spherical harmonic:[19]

$$I_{J,M,\gamma}(\hat{\boldsymbol{R}}, \hat{\boldsymbol{r}_1}, \hat{\boldsymbol{r}_2}) = \sum_{m_1 m_2 m_{12} M_{L_{end}}} C^{j_{12}m_{12}}_{j_1 m_1 j_2 m_2} C^{JM}_{j_{12}m_{12}L_{end}M_{L_{end}}} Y_{j_1,m_1}(\hat{\boldsymbol{r}_1})$$

$$\times Y_{j_2,m_2}(\hat{\boldsymbol{r}_2}) Y_{L_{end},M_{L_{end}}}(\hat{\boldsymbol{R}}) \tag{3.3}$$

In the above equation, ν_1 and ν_2 and j_1 and j_2 indicate the vibrational state and rotational angular momentum associated with each individual monomer.[50] L_{end} represents the angular momentum associated with the end-over-end rotation (n.b. we have used L_{end} instead of the regular notation L to distinguish it from the potential energy index L described below). To better explore this model, it is worthwhile to consider each of the components separately. Since we have already discussed $\hat{h}_1$ and $\hat{h}_2$, we consider next the potential energy operator in the space-fixed representation.[39] Note that we choose a space-fixed representation of the wavefunction in order to allow for a better comparison between our results and previous studies presented by Hinde and McKellar. In addition, the use of a space-fixed representation for the dimer system allows for a clearer extension to a multi-dimer system in future work, where a body-fixed representation is not appropriate. We note that:

$$\hat{V}_{12} = \sum_{l_1,l_2,L} \hat{A}_{l_1,l_2,L}(R, r_1, r_2) \hat{G}_{l_1,l_2,L}(\hat{\boldsymbol{R}}, \hat{\boldsymbol{r}_1}, \hat{\boldsymbol{r}_2}) \tag{3.4}$$

Where:[39]

$$\hat{G}_{l_1,l_2,L}(\hat{\boldsymbol{R}},\hat{\boldsymbol{r}}_1,\hat{\boldsymbol{r}}_2) = \sum_{m_{l_1} m_{l_2} m_L} C^{Lm_L}_{l_1 m_{l_1} l_2 m_{l_2}} Y_{l_1,m_{l_1}}(\hat{\boldsymbol{r}}_1) Y_{l_2,m_{l_2}}(\hat{\boldsymbol{r}}_2) Y_{L,m_L}(\hat{\boldsymbol{R}})^* \qquad (3.5)$$

We determine the matrix elements of $\hat{V}_{12}$ by integrating through the radial monomer and angular wavefunctions. Note that these matrix elements are diagonal with respect to the radial dimer wavefunction, which we include in the final equation for the total matrix elements:

$$\langle\lambda|\,\hat{V}_{12}\,|\lambda'\rangle = \sum_{l_1,l_2,L} \langle\nu_1 j_1 \nu_2 j_2|\,\hat{A}_{l_1,l_2,L}\,|\nu_1' j_1' \nu_2' j_2'\rangle\,\langle\gamma JM|\,\hat{G}_{l_1,l_2,L}\,|\gamma' J'M'\rangle \qquad (3.6)$$

In line with past work, we only consider the four most important angular expansions relevant for the $(H_2)_2$ dimer, with the following l_1, l_2, and L values: G_{000}, G_{022}, G_{202}, and G_{224}.[16,19,51] The first part of each matrix element must be integrated numerically (i.e. numerical quadrature) using the calculated monomer wavefunctions from before, producing a matrix element for each $A_{l_1,l_2,L}$ term that varies with R. However, the second part can be solved analytically, by integrating over the monomer and dimer angular components. We include the final, derived expression below.[37–40] Note that after integration, the matrix elements are revealed to be all real-valued:

$$\langle\lambda|\,\hat{V}_{12}\,|\lambda'\rangle = \sum_{l_1 l_2 L} \langle\nu_1 j_1 \nu_2 j_2|\,\hat{A}_{l_1,l_2,L}\,|\nu_1' j_1' \nu_2' j_2'\rangle\,(-1)^{J+j_1+j_2+j_{12}'}$$

$$\times \left([L]^2 [l_1][l_2][j_1][j_2][j_{12}][L_{end}][j_1'][j_2'][j_{12}'][L_{end}']\right)^{1/2}$$

$$\times \begin{pmatrix} L & L_{end}' & L_{end} \\ 0 & 0 & 0 \end{pmatrix} \begin{pmatrix} l_1 & j_1' & j_1 \\ 0 & 0 & 0 \end{pmatrix} \begin{pmatrix} l_2 & j_2' & j_2 \\ 0 & 0 & 0 \end{pmatrix}$$

$$\times \begin{Bmatrix} L'_{end} & L_{end} & L \\ j_{12} & j'_{12} & J \end{Bmatrix} \begin{Bmatrix} j'_{12} & j'_2 & j'_1 \\ j_{12} & j_2 & j_1 \\ L & l_2 & l_1 \end{Bmatrix} \delta_{J,J'} \delta_{M,M'} \qquad (3.7)$$

In the above equation, $\langle \nu_1 j_1 \nu_2 j_2 | \hat{A}_{l_1,l_2,L} | \nu'_1 j'_1 \nu'_2 j'_2 \rangle$ represents the vibrationally averaged radial coefficients, and takes into account the $(4\pi)^{-3/2}$ term explicitly written out in the above equation by Green. Note that $[x] = 2x + 1$, and that the various parentheses are used to indicate 3-j, 6-j, and 9-j Wigner symbols. We see from the above equation that the matrix elements are diagonal in J and independent of M; we therefore do not need to include the M term in the final version of the matrix element equations. Matrix channels with different parities (i.e. $(-1)^{J+j_1+j_2+L_{end}} \neq (-1)^{J+j'_1+j'_2+L'_{end}}$) do not couple together and can be treated separately. The resulting equation is also implicitly independent of the terms m_1, m_2, $M_{L_{end}}$, and m_{12} as a result of symmetry gained through the use of higher order Wigner symbols. These ideas allow for a considerable reduction in both the overall basis size and computational time required for the calculation of the matrix elements. In line with Hinde's method, for this work, we restrict both j_1 and j_2 to values of 0, 2, 4 (para hydrogen, ortho deuterium, or para tritium) or 1, 3, 5 (ortho hydrogen, para deuterium, or ortho tritium). However, we do not truncate the basis for the total allowed value of $j_1 + j_2$ as Hinde does. Using this expanded basis for j_1 and j_2, the maximum value of j_{12} is 8, 9, and 10 for pH_2-pH_2, oH_2-pH_2, and oH_2-oH_2 hydrogen dimers, respectively [the opposite order is true for $(D_2)_2$]. This consideration allows us to determine the maximum allowed L_{end} value that produces

non-zero values, since:

$$|L'_{end} - j'_{12}| \leq J \leq L'_{end} + j'_{12} \tag{3.8}$$

$$|L_{end} - j_{12}| \leq J \leq L_{end} + j_{12} \tag{3.9}$$

Since $j_{12,max} = j'_{12,max}$, we see that $L_{end,max} = L'_{end,max} = j_{12,max} + J$, which provides us additional information about the size of our basis being employed. For the kinetic energy operator $\hat{T}_R$, we begin by writing the operator in the following form:

$$\hat{T}_R = -\frac{\hbar^2}{2\mu_{AB}R^2}\frac{\partial}{\partial R}\left(R^2\frac{\partial}{\partial R}\right) + \frac{1}{2\mu_{AB}R^2}\hat{L}^2_{end} \tag{3.10}$$

We employ a numerical method known as as the Colbert-Miller Discrete Variable Representation (CM-DVR)[52] that relies on a grid composed of evenly spaced radial points (a), such that $\Delta R = \frac{R_{max}-R_{min}}{N}$ and $R_a = R_{min} + a\Delta R$, where a ranges from 1 to $N-1$.[53] Note that the kinetic energy converges in value as the space between the grid points decreases. We can therefore rewrite our matrix elements within the a grid as:

$$
\begin{aligned}
\langle a\lambda| \, \hat{H} \, |a'\lambda'\rangle &= \langle a\lambda| \, \hat{T}_R + \hat{h}_1 + \hat{h}_2 + \hat{V}_{12} \, |a'\lambda'\rangle \\
&= \Big[\langle a| \, \hat{T}_{rad} \, |a'\rangle + \frac{\hbar^2}{2\mu_{AB}R_a^2}(L_{end})(L_{end}+1)\delta_{aa'}\Big]\delta_{\lambda\lambda'} + E^{v_1}_{j_1}\delta_{\lambda\lambda'}\delta_{aa'} \\
&\quad + E^{v_2}_{j_2}\delta_{\lambda\lambda'}\delta_{aa'} + \langle\lambda| \, \hat{V}_{12} \, |\lambda'\rangle \, \delta_{aa'}
\end{aligned}
\tag{3.11}
$$

Where:

$$\langle a | \hat{T}_{rad} | a' \rangle = \frac{\hbar^2}{2\mu_{AB}\Delta R^2}(-1)^{a-a'} \begin{cases} \frac{\pi^2}{3} - \frac{1}{2a^2} & a = a' \\ \\ \frac{2}{(a-a')^2} - \frac{2}{(a+a')^2} & a \neq a' \end{cases} \tag{3.12}$$

We compute the Wigner symbols using the built-in functions provided by the SymPy package on Python.[54,55] The resulting eigenvalues for this matrix are determined using an efficient eigenvalue solver (ARPACK) to find the lowest (smallest algebraic, i.e. most negative in value) binding states,[56] labeled with the five quantum numbers $(j_1, j_2, j_{12}, J, L_{end})$. Of these five quantum numbers, only J is considered to be 'good'. The remaining four are approximations that include contributions from other states. Note that the exact number of states that exist is difficult to predict in advance and is obtained here by the presence of negative binding energies. The states included throughout this paper are referred to as "ground states", since they consist of contributions primarily from the lowest para $(j = 0)$ or ortho $(j = 1)$ states. In particular, coupling is high between states that share four out of the five same quantum numbers. We generally are able to label our binding energy results without much difficulty, using the largest basis contribution for each calculated eigenfunction and arriving at similar results to those obtained by McKellar.[11,12] However, McKellar finds that the binding energy associated with ortho-ortho hydrogen's $(1, 1, 2, 1, 1)$ state has a higher (more positive) value than that associated with the $(1, 1, 0, 1, 1)$ state. In comparison, in our calculations, it appears that the opposite is true. Although this is not explicitly discussed by McKellar, more recent investigations[57] suggest that there is a convention for labeling states that share four out of the five same quantum numbers and experience significant coupling: binding energies become more positive with increasing j_{12} and L_{end}. For our calculations, we

do not assume that this assumption is correct and retain the original, largest contributions to the eigenfunctions without any additional sorting. For the deuterium and tritium dimers, we also maintain this approach due to more complicated coupling schemes and scenarios where both L_{end} and j_{12} change.

3.1.2   Symmetry of $(H_2)_2$ and $(D_2)_2$

The symmetry of $(H_2)_2$ has been extensively explored in the literature[40,58,59] and serves as a useful means of explaining some of the spectral properties of the dimer. We assume that the rovibrational wavefunction (Ψ_{rv}) can be approximated as the product of components of vibrational (ν_1, ν_2, n) and rotational (j_1, j_2, L_{end}) quantum numbers:

$$\Psi_{rv} = |\nu_1\nu_2\pm\rangle |j_1j_2\pm\rangle |n\rangle |L_{end}\rangle \tag{3.13}$$

In the above equation, note the following non-normalized relationships:[58]

$$|\nu_1\nu_2\pm\rangle = \Phi_{\nu_1}(r_1)\Phi_{\nu_2}(r_2) \pm \Phi_{\nu_1}(r_2)\Phi_{\nu_2}(r_1) \tag{3.14}$$

$$|j_1j_2\pm\rangle = Y_{j_1,m_1}(\hat{\boldsymbol{r}}_1)Y_{j_2,m_2}(\hat{\boldsymbol{r}}_2) \pm Y_{j_1,m_1}(\hat{\boldsymbol{r}}_2)Y_{j_2,m_2}(\hat{\boldsymbol{r}}_1) \tag{3.15}$$

Each basis wavefunction can be described by a particular symmetry under certain conditions, as outlined in Table 3 from Bunker.[58] After noting the nuclear spin statistics for para (1 state, even j values) and ortho hydrogen (3 states, odd j values) monomers, we treat each molecule as a 'single particle' in a dimer system, with molecular symmetry $\boldsymbol{G}_{16}$. Although a full discussion of the chosen symmetry scheme will not be provided here, $\boldsymbol{G}_{16}$ is a convenient

method of describing sixteen different possible exchanges of the four hydrogen nuclei, with the caveat that the intramolecular bonds of the two hydrogen monomers are never broken. In the case of pH_2-oH_2 or oH_2-pH_2, the particles are distinguishable, with nuclear spin symmetry $^3E^+$, while pH_2-pH_2 and oH_2-oH_2 consist of indistinguishable particles. The actual geometry of the hydrogen dimer has been a challenging area of research, with a recent study suggesting energetically favourable minima for linear, symmetric top, and spherical top geometries.[60] For the pH_2-pH_2 dimer, a total nuclear spin of 0 is possible, with allowed nuclear spin symmetry $^1B_1^+$. By contrast, the oH_2-oH_2 dimer may have possible total nuclear spin values of 0, 1, and 2 with permitted nuclear spin symmetries $^1A_1^+, {}^3B_2^+, {}^5A_1^+$.[12,58] The final symmetry can be shown to be restricted to B_1^+ and A_1^- symmetries, using the character table for $\boldsymbol{G}_{16}$.[58] Both of these states are antisymmetric upon exchange of each individual hydrogen nucleus within a molecule (fermions), but symmetric upon exchange of the two hydrogen molecules with each other (bosons). This analysis permits the assignment of nuclear spin statistics. For pH_2-pH_2, there is always a ratio of 1 symmetric: 0 antisymmetric nuclear spin states, while for oH_2-oH_2, a ratio of 6 symmetric: 3 antisymmetric spin states remains constant. Note that the antisymmetric and symmetric eigenstates are the same as the symmetric and antisymmetric oH_2-oH_2 labels used in Table 3 by McKellar and Schaefer.[12] Furthermore, for non-identical oH_2-pH_2 and pH_2-oH_2 dimers, there is a nuclear statistical weight of 6 (3+3) relative to the other terms. A similar analysis can be performed for the $(D_2)_2$ dimer, with ortho (6 states, even j values) and para (3 states, odd j values) nuclear spin isomers. Here, oD_2-oD_2 has a ratio of 21 symmetric: 15 antisymmetric nuclear spin states.[12] In contrast, pD_2-pD_2 has a ratio of 6 symmetric: 3 antisymmetric nuclear spin states, while pD_2-oD_2 and oD_2-pD_2 have a combined nuclear weight of 36 (18+18). In comparison to hydrogen,

the deuterium nuclei are bosons and are symmetric upon exchange. This property leads to allowed final symmetries only of A_1^+ and B_1^- character. Note that $(T_2)_2$ has the same nuclear spin statistics as $(H_2)_2$, since $I_T = I_H = \frac{1}{2}$.[61] While there are different methods of determining symmetry of our eigenstates, we use a standard approach by symmetrizing the wavefunctions for our system for identical particles.[12] In particular, the final expression allows us to separate our matrices into symmetric and antisymmetric blocks for cases where the dimer consists of identical particles:[40,46]

$$\langle \lambda | \hat{V}_{12} | \lambda' \rangle^{\pm} = [(1 + \delta_{\nu_1 \nu_2} \delta_{j_1 j_2})(1 + \delta_{\nu_1' \nu_2'} \delta_{j_1' j_2'})]^{-\frac{1}{2}} [\langle \lambda | \hat{V}_{12} | \lambda' \rangle$$

$$\pm (-1)^{j_1 + j_2 - j_{12} + L_{end}} \langle \lambda_{sym} | \hat{V}_{12} | \lambda' \rangle] \tag{3.16}$$

Where, from before, $\lambda = (\nu_1 \nu_2 j_1 j_2 j_{12} L_{end} J)$ and now $\lambda_{sym} = (\nu_2 \nu_1 j_2 j_1 j_{12} L_{end} J)$. For identical particles, we are also able to further restrict the basis λ to only include cases where $\nu_1 < \nu_2$ or $\nu_1 = \nu_2$ and $j_1 \leq j_2$. Note that the equation given above follows the form derived previously (refer to Eq. 56 by Takayanagi[46]), which includes the interchange of ν_1 and ν_2 omitted in the final potential expression by Schaefer and Meyer[40] (refer to Eq. 12 given in the source). In addition, we are able to reduce the basis size further by separating out certain symmetrical and antisymmetrical rotational functions. Consider first that when $j_1 = j_2$, $|j_1 j_1 +\rangle$ can only have even j_{12}, while $|j_1 j_1 -\rangle$ can only have odd j_{12} values.[59] Furthermore, when $\nu_1 = \nu_2$, only $|\nu_1 \nu_1 +\rangle$ terms exist (with A_1^+ symmetry), and consequently, the value of the rotational phase factor $(-1)^{j_1 + j_2 - j_{12} + L_{end}} = (-1)^{-j_{12} + L_{end}}$ determines whether or not a state is symmetric or antisymmetric.[40] For instance, a ground vibrational state $(j_1, j_2, j_{12}, J, L_{end}) = (1, 1, 0, 1, 1)$ is antisymmetric while $(1, 1, 1, 1, 1)$ is symmetric and can

be treated separately in our matrix calculations. Our final eigenvalues are therefore able to be sorted in terms of symmetric and antisymmetric rovibrational functions, with allowed and forbidden nuclear spin symmetries determined using the method described above.

3.1.3 Summary of Allowed Transitions for IR and Raman spectroscopy

As a means of comparison, the selection rules for electric dipole-infrared spectroscopy have been derived previously,[58] with the conditions requiring that $\Delta L_{end} = odd$, $\Delta J = 0, \pm 1$.[62–64] Nuclear spin statistics must also be considered in determining the relative intensity of each of the spectral lines for the different dimer species. For vibrational IR excitations, the above selection rules demand that transitions occur from the ground state to the excited state in which the vibration is delocalized antisymmetrically (i.e. $|\nu_1\nu_2-\rangle$).[19] While the simple cases of pH_2-pH_2 and oD_2-oD_2 have a limited number of accessible ground states, other spin isomers have many different ground states that may undergo vibrational excitations. For vibrational Raman spectroscopy of these dimers, previous studies[19,22,23] have focused on pure vibrational Q(0) and Q(1) lines, in which $\Delta v = \pm 1$ and $\Delta j_1, \Delta j_2 = 0$. In the vibrational Raman spectrum for isolated hydrogen molecules, these transitions occur only for the case $\nu = 1 \leftarrow 0$, J←J.[5] For dimers, the individual angular momenta of each hydrogen molecule couples with the end-over-end rotation of the dimer to produce J. If the overall selection rules are the same as for rovibrational lines in diatomic molecules ($\Delta J = 0, \pm 2$), there may be additional lines in the Q-branch for ortho-ortho hydrogen. This idea was suggested by Hinde[19] for several predicted ortho-ortho deuterium dimer Raman lines despite there being

no change in j_1 or j_2. However, the actual existence and intensity of $\Delta J = \pm 2$ lines within the Q region remains unknown and cannot be verified with the current state of Raman vibrational spectroscopy available for the dimers in question. In addition, individual hydrogen molecules exhibit very weak anisotropic contributions in their vibrational Raman spectrum that are usually neglected for much stronger isotropic scattering that is independent of the total angular momentum J.[5] Past studies involving the polarizability of the hydrogen dimer have indicated that the complex exhibits both isotropic and anisotropic changes as a consequence of molecular scattering.[65,66] A full analysis of the polarizability operator, composed of the individual molecular and dimer polarizability changes, will not be explored here. For our present work, we consider only isotropic scattering and we assume here that any change in this property associated with the dimers colliding is insignificant compared to the polarizability inherent to each molecule. If we approximate the total wavefunction (Ψ_T) as a product of $\psi_{ns}\psi_{rot}\psi_{vib}$ for a given electronic state, the selection rules demand that $\psi'_{ns} = \psi_{ns}$ and $\psi'_{rot} = \psi_{rot}$, with totally symmetric vibrational symmetry ($\Gamma'_{vib} = \Gamma_{vib}$).[59] While the quantum number labels included in the tables in Section 3.2 for j_1, j_2, j_{12}, and L_{end} are approximate, we use them to only consider 'pure' Q lines, i.e. those in which the initial and final states share the same five values with the inclusion of the good quantum number J. This assumption allows us to significantly restrict the number of possible transitions and compare our results more easily to available experimental findings. As we described in the following sections, our relative line intensities are approximated using a combination of Boltzmann and nuclear spin statistics.

3.1.4 Computational Details

For both computational efficiency and utility, a variety of tools are used in the construction of the resulting software. The bulk of the code, responsible for generating and storing matrix elements is written in C++, with a wrapper function used to call Hinde's 6D Fortran code to obtain the A coefficients. We make use of two Python libraries in our code, as mentioned previously: (1) SymPy[54,55] is used to generate relevant Wigner 3j, 6j, and 9j coefficients in our analytical G component of the matrix elements and (2) SciPy's[56,67] implementation of ARPACK is used to obtain the resulting binding energies as generated eigenvalues. Both Python libraries are used such that objects are passed back and forth using a Python/C API mechanism to embed short Python functions. This setup allows for the more computationally expensive length of the code to run more efficiently in the compiler-based C++ language, while making use of well-supported libraries in Python. For SciPy's ARPACK code, we make use of default settings (i.e. number of iterations is total basis size times 10, tolerance is set at machine precision, etc.) We choose to obtain the thirty lowest eigenvalues of our produced sparse matrices using the "SA" (smallest algebraic) feature of ARPACK and only include values with negative values that represent our bound binding states. Larger matrices tend to experience more difficulty in converging, requiring more computational time and iterations. However, alternative setups involving the "LM" (largest magnitude) setting with appropriate shifts of the diagonal of our matrices do not reveal any significant differences in reported results. For completion, we include a table summarizing the Basis Set used in our final calculations (Table 3.1). Note that in our case, we supply sparse matrices to ARPACK for eigenvalue calculations, but matrix vector products are also possible inputs to the software.

Table 3.1: Parameters used in the Construction of Basis Set

$j_{para,max}$	$j_{ortho,max}$	J	$L_{end,max}$	DVR$_{grid}$ (spacing)	Parity	Symmetry (id. particles)
4	5	0, 1, 2, 3, 4	$j_{12,max} + J$	3.0-48.0 a_0 (0.05 a_0)	$(-1)^{j_1+j_2+L_{end}+J}$	$\nu_1 < \nu_2$ or ($\nu_1 = \nu_2$ and $j_1 \leq j_2$)

Table 3.2: Rovibrational energies values calculated from LEVEL[49] code

ν	j	H$_2$ (cm^{-1})	D$_2$ (cm^{-1})	T$_2$ (cm^{-1})
0	0	-36117.5942855	-36748.1782171	-37028.3869532
0	1	-35999.1009407	-36688.3959347	-36988.3231995
0	2	-35763.2015637	-36569.1061141	-36908.3186562
0	3	-35412.0362763	-36390.8538543	-36788.6179323
0	4	-34948.7315935	-36154.4459969	-36629.5846922
0	5	-34377.3069200	-35860.9386127	-36431.6978427
1	0	-31955.5931841	-33754.2565798	-34563.7140808
1	1	-31843.0132054	-33696.5845329	-34524.8061821
1	2	-31618.9043026	-33581.5086500	-34447.1109509
1	3	-31285.3346870	-33409.5610143	-34330.8682121
1	4	-30845.3245590	-33181.5290728	-34176.4344847
1	5	-30302.7545620	-32898.4432846	-33984.2792069

3.2   Results

We compute the binding energies for (H$_2$)$_2$, (D$_2$)$_2$, and (T$_2$)$_2$ by determining the first few eigenvalues of the matrices described above and subtracting the relevant monomer energies ($E_{\nu_1 j_1}$, $E_{\nu_2 j_2}$). For completion, we present a short table summarizing the energies used in our calculations (Table 3.2). These values vary depending on the particular dimer combination being considered (Tables 3.3-3.5). While we attempt to maintain a consistent approach with Hinde's methods, we employ a few different corrections. In particular, we use slightly different masses for each dimer, relying on the NIST elemental database[68] and constants:[69] 3674.31 m_e, 7342.97 m_e, and 10995.84 m_e for the three isotopologues, respectively. Note

that in all three tables, the mixed dimer combinations (i.e. consisting of one ortho and one para molecule) have two possible vibrational shifts dependent on selective excitation of each distinguishable molecule. We obtain our potential energy results on the same boundaries as Hinde, from 3.0 a_0 to 48.0 a_0, with smaller grid point (0.05 a_0) intervals for a total of 901 radial points to improve convergence (i.e. $R_1 = 3.0$ a_0, $R_{N-1=901} = 48.0$ a_0). Since Hinde does not recommend the use of his potential below 4.210625 a_0 in his attached Supplementary code, we cap the potential at that limit for any lower R values while still using the correct DVR grid point. We also assume that $\nu_T = \nu_1 + \nu_2 = 0$ and $\nu_T = \nu_1 + \nu_2 = 1$ do not couple and can be evaluated separately. For ortho-para dimers, we evaluate the two $\nu_T = \nu_1 + \nu_2 = 1$ states together, and find that there exists a weak coupling in the vibrational states in which either an ortho or para molecule is being excited. Our results for the hydrogen dimer binding energies are presented in the last three columns of Table 3.3. We also include McKellar and Schaefer's theoretical findings[12,20] for ground state binding energies in the column with the heading $-\boldsymbol{E}_{\nu_T=0}^{M-S}$.

Note that there are slight differences between our binding energies and those obtained by Hinde in his work involving para hydrogen and ortho deuterium, at about the third decimal place. These small deviations are likely due to different methods of obtaining the monomer rovibrational wavefunctions $\Psi_{\nu j}$, including the possible differences in the number of gridpoints used for the quadrature of the $A_{l_1,l_2,L}$ coefficients. In addition, Hinde employed a five-point central difference approximation for his kinetic energy operator instead of the DVR method that we use, which may also be responsible for the small deviation. In comparison to the results obtained by McKellar and Schaefer, our results differ at about the second

Table 3.3: Calculation of Binding Energies and Raman Shifts for ground and excited state H_2-H_2 dimers,[b] with comparison to past theoretical results.[12,20]

Nuclear Spin Symmetry	j_1	j_2	j_{12}	J	L_{end}	$-E^{M-S}_{\nu_T=0}$[12,20] (cm^{-1})	$-E^{Hinde}_{\nu_T=0}$ (cm^{-1})	$-E^{Hinde}_{\nu_T=1}$ (cm^{-1})	$-\Delta\nu$ (cm^{-1})
pH$_2$-pH$_2$, B$_1^+$ (1)	0	0	0	0	0	2.849	2.899	3.304	0.405
oH$_2$-pH$_2$, E$^+$ (3*2)	1	0	1	0	1	1.718	1.746	2.112, 2.099	0.366, 0.353
			1	1	0	2.875	2.931	3.257, 3.253	0.326, 0.322
			1	1	1	1.102	1.176	1.436, 1.442	0.260, 0.266
			1	2	1	1.353	1.408	1.713, 1.707	0.305, 0.299
Sym. oH$_2$-oH$_2$, A$_1^+$ (6)	1	1	0	0	0	2.946	2.981	3.411	0.430
			1	0	1	0.885	0.999	1.289	0.290
			1	1	1	1.505	1.553	1.968	0.415
			2	2	0	3.015	3.083	3.546	0.462
			1	2	1	1.260	1.335	1.704	0.369
Antisym. oH$_2$-oH$_2$, B$_2^+$ (3)	1	1	1	1	0	2.862	2.932	3.345	0.414
			0^a	1	1	1.234	1.288	1.661	0.374
			2	1	1	2.009	2.039	2.576	0.537
			2	2	1	1.145	1.224	1.587	0.363
			2	3	1	1.480	1.539	1.964	0.425

^{a}Literature values for the $(1,1,0,1,1)$ and $(1,1,2,1,1)$ binding energies are flipped, for consistency with the convention used in this paper.
^{b}For the mixed pair, the two vibrationally excited states correspond to the selective excitation of ortho and para hydrogen, respectively.

decimal place, likely due to the different PES employed. Using these binding energies and the corresponding calculated states with one quantum of vibration, we confirm and predict the vibrational Q(0) and Q(1) Raman shifts for the three dimers by subtracting the excited state bound energies by the ground state bound energies, with comparisons made to experimental values. At low temperatures, ground rotational states tend to be exclusively populated (i.e. $j = 0$ or $j = 1$), which we only consider here for our bound states. While para-para hydrogen has only a single ground state, $(j_1, j_2, j_{12}, J, L_{end}) = (0, 0, 0, 0, 0)$, that can be excited vibrationally, there are many possible ortho-para and ortho-ortho bound states that arise for their respective dimers. However, the Boltzmann factor $e^{-E_{\gamma,J}/k_B T}$ plays an important role in determining the population of energy states depending on the temperature being employed in the experiment. The weightings associated with the $(2J+1)$ degeneracy as well as the nuclear spin statistics (g) also contribute in determining the overall population of a given ground energy state. This approach allows us to determine the most populated states

likely responsible for the observed Raman dimer transitions. As one method of approxima-
tion, we can consider each of the bound states as capable of transitions independent of each
other, modeled using the standard Stokes vibrational Raman scattering for diatomics (refer
to Eq. 8.98 from Bernath[70]). To better explore this idea, consider a delocalized symmetric
vibrational state excited from the ground state, with polarizability operators $\alpha_1(r)$ and $\alpha_2(r)$
that can excite the first and second molecule, respectively. Note that in the equation below,
$\nu_{12} = \frac{1}{\sqrt{2}}(|\nu_a \nu_b\rangle + |\nu_b \nu_a\rangle)$. If we are exciting from the symmetric ground state $|00\rangle$, we find
that:

$$\langle \nu_{12}| \, \alpha_1(r) + \alpha_2(r) \, |00\rangle = \frac{1}{\sqrt{2}} \Big(\langle \nu_a| \, \alpha_1(r) \, |0\rangle \, \delta_{\nu_b,0} + \langle \nu_b| \, \alpha_2(r) \, |0\rangle \, \delta_{\nu_a,0}$$

$$+ \langle \nu_a| \, \alpha_2(r) \, |0\rangle \, \delta_{\nu_b,0} + \langle \nu_b| \, \alpha_1(r) \, |0\rangle \, \delta_{\nu_a,0} \Big)$$

$$= \sqrt{2} \, \langle 1| \, \alpha_1(r) \, |0\rangle \qquad\qquad (3.17)$$

For vibrational transitions, we assume a harmonic oscillator model where $\Delta v = \pm 1$ for all of
the matrix elements. If we are transitioning from an initial ground $|00\rangle$ state, $(\nu_a, \nu_b) = (1,0)$
or $(\nu_a, \nu_b) = (0,1)$. Note that the above equation is only valid for dimer pairs in which the
two molecules are indistinguishable and is very similar to the matrix element given by Van
Kranendonk[5] (refer to Eq 3.106 in the source) for the Raman amplitude of solid hydrogen
vibrational delocalization. This approximation assumes that: (a) similar to isolated hydrogen
molecules, the polarizability operator is independent of the value of j_1, j_2 (i.e. equal for both
ortho and para hydrogen) and (b) the eigenstates are composed of a single bound state.[5]
In practice, coupling between various quantum states lowers the accuracy of the labeling
system employed; this model of polarazibility will require additional considerations when

higher resolution experimental spectra are produced. In line with this assumption, the frequency of transition is very similar for all of the possible transitions (about 4155.25 cm^{-1} for Q(1) and 4161.18 cm^{-1} for Q(0) as given previously[30]), since the Raman shifts that arise from the intermolecular interactions are generally less than -0.5 cm^{-1}. Note as well that all of the excited first vibrational states are unpopulated at the low temperatures performed in this experiment. Therefore, we assume that the only significant factors responsible for determining the strength of the transition are the relative population of the ground bound states (based on the dimer ground state energy $E_{\gamma,J}$), nuclear spin weight (g), and $(2J+1)$ rotational degeneracy mentioned above (associated with the M_J projection of each dimer state). These three important considerations were subsequently added to our equation. These ideas are also explored by Bunker, in his equation for the transition probability of isotropic Raman scattering (14-136).[59] In summary, we exclusively focus on the relative populations of each dimer pair's states, such that this quantity is calculated at a given temperature T for each set of calculations. Note as well that in the equation below k_b is the Boltzmann constant (0.6950348004 cm$^{-1}/K$).

$$p_{\gamma_i,J_i} = \frac{g_i(2J_i+1)e^{-E_{\gamma_i,J_i}/k_BT}}{\sum_{i=1}^{N} g_i(2J_i+1)e^{-E_{\gamma_i,J_i}/k_BT}} \tag{3.18}$$

For instance, for oH$_2$-oH$_2$, the symmetric state $(j_1, j_2, j_{12}, J, L_{end}) = (1,1,2,2,0)$ has both the lowest ground vibrational energy state and a $(2J+1)$ degeneracy of 5. Along with a symmetric nuclear spin weight of 6, this state would be expected to play the dominant role in the vibrational Q(1) transition, particularly at low temperatures where the state is exclusively populated. However, as the temperature increases, other states begin to exhibit

43

increased population and contribute to the Raman peak as the Boltzmann factor becomes less important in comparison to nuclear spin statistics and rotational degeneracy. This consideration allows us to calculate a change in Raman shift from a high of about -0.460 cm^{-1} at 0.1 K to a converged shift of -0.416 cm^{-1} at 10.0 K, which is closer in magnitude to the approximate reported shift of -0.4 cm^{-1} by Montero et al. The paper also reported a more specific ratio of about $\sqrt{2}$ for the oH_2-oH_2 and oH_2-pH_2 shifts. Although this value was presented without additional clarification by Montero et al., it remains a good match for our observed results at all temperatures within the uncertainty associated with the experimental shifts. We present our data in two different ways: using a predicted vibrational spectrum with the relative intensities calculated above (Figure 3.1) or as a weighted average based on relative intensity (Figure 3.2), that attempts to predict the wavenumber of the dominant peak at different temperatures. Note that the location of our obtained spectral peaks are found by adding the negative Raman shift to Q(0) and Q(1) monomer lines given by Montero et al.[30] for $(H_2)_2$ dimers. For comparison, the experimental Raman shifts appear as dashed lines in our spectra using the approximate dotted lines and shifts given in the paper. This choice is made since the monomer vibrational transitions calculated by the LEVEL code appear to be slightly blue-shifted from experimental values as the final energy eigenvalues lack non-adiabatic corrections; while this appears to have a minimal effect on the calculated bound energy states and obtained Raman shifts, it produces incorrect vibrational peaks for the purposes of comparison on a single spectrum. For the $(D_2)_2$ and $(T_2)_2$ dimers, we use experimentally obtained Q(0) and Q(1) lines.[71,72] The results we present assume that the hydrogen dimers were formed at equilibrium conditions (i.e. $3oH_2:1pH_2$, $2oD_2:1pD_2$, $3oT_2:1pT_2$). Although the exact local temperature is not given, we cool the dimers to a
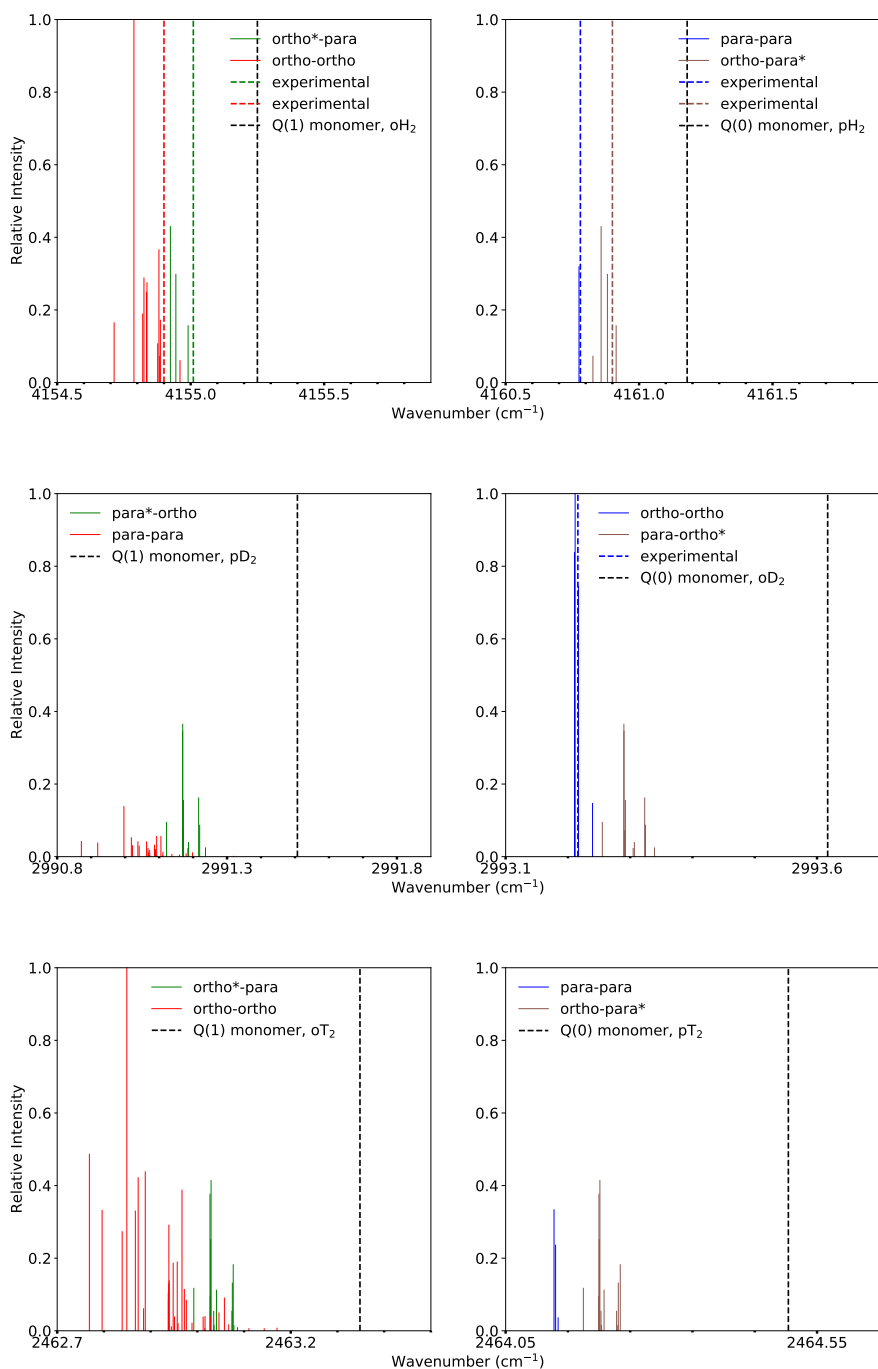
Figure 3.1: Calculated Q(0) and Q(1) Vibrational Spectrum of $(H_2)_2$ dimer (top) and its isotopologues $(D_2)_2$ (centre) and $(T_2)_2$ (bottom) at 2.5 K using a Boltzmann Weighting Factor, Nuclear Spin Statistics, and $(2J+1)$ rotational degeneracy. All positions are calculated relative to the experimental vibrational energies.[30,71,72] We also include the approximate experimental shifts obtained from the spectra provided by Montero et al.,[30] as a shift from the dominant Q(0) and Q(1) monomer lines for the $(H_2)_2$ dimer. The experimental ortho-ortho deuterium shift was also obtained previously[23] and is also included here for comparison.
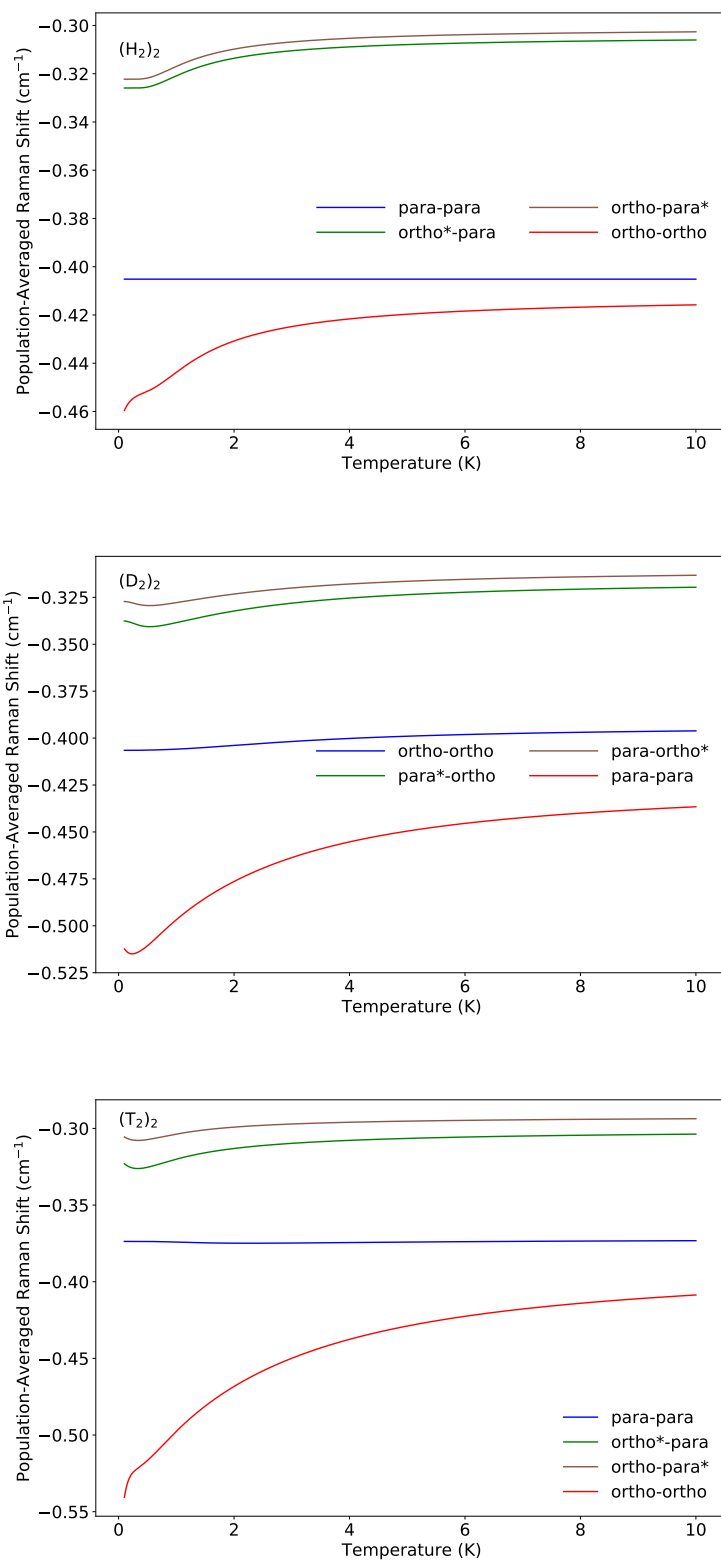
Figure 3.2: Calculated Population-Averaged Raman Shifts from Q(0) and Q(1) lines of $(H_2)_2$ dimer (top) and its isotopologues $(D_2)_2$ (centre) and $(T_2)_2$ (bottom), from 0.1 to 10 K (in 0.01 K intervals). All shifts are calculated relative to the monomer vibrational energies produced by the LEVEL code.[49]

46

temperature of 2.5 K based on the parameters and temperatures reported previously.[21] It is also assumed that interconversion between spin isomers is no longer possible during the cooling process. We multiply the calculated relative populations by the nuclear spin weight at equilibrium (e.g. 9 for oH_2-oH_2 , 3x2 for oH_2-pH_2 and pH_2-oH_2, and 1 for pH_2-pH_2). Note that the total intensity should satisfy the principle of spectroscopic stability for ortho-para combinations, in which the total intensity of the system remains constant for any dimer pair.[5] In particular, we assume that the total intensity of the two ortho-para peaks is equivalent to the intensity that would exist for a dimer pair with two indistinguishable particles that produces a single peak. Due to the lack of delocalization, each separate ortho-para peak is consequently an additional 0.5 times weaker based on the polarizability terms defined above. However, when we include the equivalent number of 'para-ortho' dimers that also form, this 0.5 factor is eliminated since the nuclear spin weighting effectively doubles. Ultimately, the overall purpose of these calculations are not to conclusively establish all of the possible transitions that may occur in the spectra, but rather explore features associated with the nature of the observed peaks. Further discussions relating to the actual shape of this peak, linewidth, and overall intensity will be reserved for a more complete discussion of polarizability in future work, some of which may be based on past work involving the intensity of the IR spectra of hydrogen dimers.[53,73,74] For the ortho-ortho and ortho-para hydrogen dimers, our Raman peaks appear to be slightly red-shifted from the obtained experimental intensity, with larger vibrational shifts. However, the relatively low spectral resolution of 0.12 cm^{-1} makes it difficult to distinguish peaks between the various dimers on the spectrum. Consequently, higher resolution spectra, akin to the vibrational IR results obtained previously by McKellar[11] with spectral resolution of 0.04 cm^{-1}, will be required to more

definitively assess the accuracy of this model for Raman spectroscopy. Nevertheless, as a first approach, the results obtained from this method are very encouraging, as they illustrate the same degree of vibrational shifts for the different spin isomers. This same approach can be applied for the $(D_2)_2$ and $(T_2)_2$ dimers; however, these dimers have additional binding states. While $(H_2)_2$ only has bound energy states up to $L_{end} = 1$, previous findings suggests that $(D_2)_2$ has bound states up to $L_{end} = 3$,[11] which we have been able to confirm using our calculated binding energies. $(T_2)_2$ adds further complexity by allowing certain bound states up to $L_{end} = 4$. For our purposes, we only consider states up to and including $J = 4$ in the determination of our spectra (higher ground J states exist in theory,[12] but are not considered here). However, many of these states are not populated at the low temperatures that we consider for Raman spectroscopy. In particular, note that Tables 3.4 and 3.5 only contain binding energies with relative ground populations of at least 2% at 2.5 K for ease of presentation of our results. We see that the corresponding mixed dimers for the deuterium and tritium dimers exhibit the lowest Raman shift as before for the hydrogen dimer, since the vibration cannot be delocalized over the two monomers as for the para-para and ortho-ortho pairs. To better illustrate the small effect that coupling has on the mixed dimers, we include additional figures showing the increased splitting associated with the Boltzmann population averaged Raman shift for all three mixed dimers (Figure 3.3). There also appears to be an increasing difference between the shifts for para-para and ortho-ortho dimers for deuterium and tritium, as compared to the hydrogen dimers. Whether or not this is a realistic result remains unknown, as this finding may be a limitation of the assumptions employed in this model. As seen previously, other states become increasingly important as the temperature increases. In particular, the 'bump' at low temperatures within the para-para deuterium

Table 3.4: Calculation of Binding Energies and Raman Shifts for ground and excited state D_2-D_2 dimers[a]

Nuclear Spin Symmetry	j_1	j_2	j_{12}	J	L_{end}	$-E$ $(cm^{-1})^{Hinde}_{\nu_T=0}$ (literature[12])	$-E$ $(cm^{-1})^{Hinde}_{\nu_T=1}$	$-\Delta\nu$ (cm^{-1})
Sym. oD_2-oD_2, A_1^+ (21)	0	0	0	0	0	6.714 (6.844)	7.121	0.407
			0	2	2	3.713 (3.816)	4.113	0.400
Antisym. oD_2-oD_2, B_2^+ (15)	0	0	0	1	1	5.698 (5.818)	6.103	0.405
			0	3	3	0.887 (0.964)	1.265	0.378
pD_2-oD_2, E^+ (18*2)	1	0	1	0	1	6.367	6.752, 6.728	0.385, 0.362
			1	1	0	6.808	7.146, 7.135	0.338, 0.327
			1	1	1	5.394	5.684, 5.687	0.291, 0.294
			1	1	2	3.970	4.306, 4.296	0.336, 0.326
			1	2	1	5.824	6.162, 6.151	0.338, 0.327
			1	2	2	3.422	3.709, 3.714	0.288, 0.293
			1	3	2	3.847	4.182, 4.172	0.336, 0.325
			1	4	3	1.013	1.334, 1.323	0.321, 0.310
Sym. pD_2-pD_2, B_1^+ (6)	1	1	0	0	0	6.900	7.340	0.440
			1	1	1	6.034	6.478	0.444
			2	1	2	6.068	6.704	0.636
			2	2	0	7.265	7.775	0.511
			1	2	1	5.682	6.096	0.414
			1	2	1	5.682	6.084	0.402
			0	2	2	3.863	4.280	0.418
			2	3	2	3.965	4.431	0.466
			2	4	2	4.132	4.602	0.470
Antisym. pD_2-pD_2, A_2^+ (3)	1	1	1	1	0	6.784	7.205	0.421
			0	1	1	5.762	6.196	0.435
			2	1	1	7.087	7.675	0.588
			2	2	1	5.824	6.309	0.485
			2	3	1	6.192	6.681	0.489

[a]Theoretical literature results [12] are available for ortho-ortho dimers and provided in parentheses. Note that for the mixed pair, the two vibrationally excited states correspond to the selective excitation of para and ortho deuterium, respectively.

Table 3.5: Calculation of Binding Energies and Raman Shifts for ground and excited state T_2-T_2 dimers[a]

Nuclear Spin Symmetry	j_1	j_2	j_{12}	J	L_{end}	$-E$ $(cm^{-1})_{\nu_T=0}^{Hinde}$	$-E$ $(cm^{-1})_{\nu_T=1}^{Hinde}$	$-\Delta\nu$ (cm^{-1})
pT_2-pT_2, B_1^+ (1)	0	0	0	0	0	8.995	9.369	0.374
			0	2	2	6.801	7.177	0.376
			0	4	4	1.895	2.264	0.370
oT_2-pT_2, E^+ (3*2)	1	0	1	0	1	9.045	9.401, 9.375	0.356, 0.329
			1	1	0	9.165	9.486, 9.469	0.321, 0.304
			1	1	1	7.902	8.174, 8.172	0.271, 0.270
			1	1	2	7.056	7.363, 7.352	0.307, 0.296
			1	2	1	8.443	8.762, 8.746	0.319, 0.303
			1	2	2	6.450	6.723, 6.723	0.273, 0.273
			1	2	3	4.890	5.203, 5.191	0.313, 0.301
			1	3	2	6.988	7.308, 7.292	0.320, 0.304
			1	3	3	4.316	4.591, 4.592	0.274, 0.276
			1	4	3	4.841	5.162, 5.146	0.321, 0.305
Sym. oT_2-oT_2, A_1^+ (6)	1	1	0	0	0	9.258	9.667	0.408
			1	1	1	8.650	9.059	0.409
			2	1	2	9.542	10.121	0.579
			2	2	0	9.908	10.407	0.499
			1	2	1	8.260	8.641	0.381
			0	2	2	6.987	7.387	0.400
			2	3	2	7.395	7.876	0.481
			2	4	2	7.451	7.911	0.460
Antisym. oT_2-oT_2, B_2^+ (3)	1	1	1	1	0	9.107	9.498	0.391
			0	1	1	8.440	8.849	0.409
			2	1	1	10.081	10.633	0.552
			2	2	1	8.855	9.364	0.509
			2	3	1	9.026	9.501	0.475
			1	3	2	6.750	7.126	0.376

[a]Note that for the mixed pair, the two vibrationally excited states correspond to the selective excitation of ortho and para tritium, respectively.
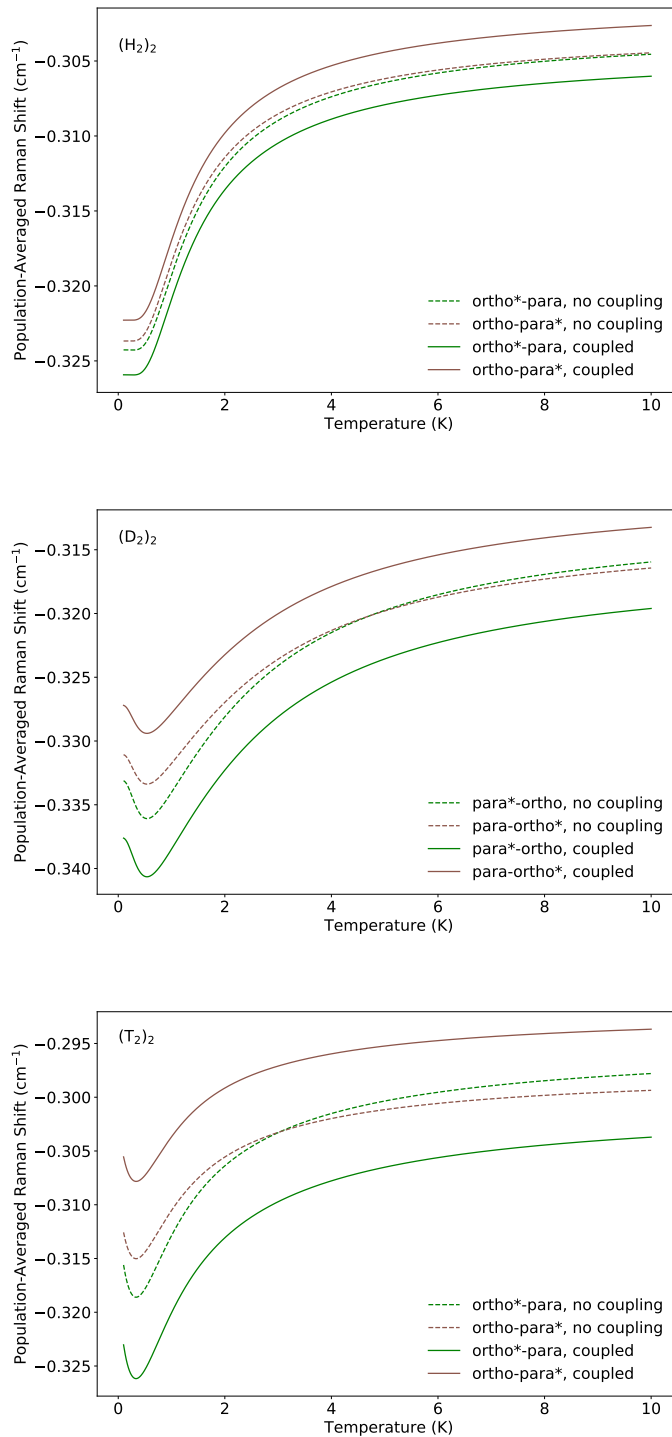
Figure 3.3: Comparison of the influence of coupling associated with the selective excitation of each component of the mixed-pair dimers for the Population-Average Raman Shift, for $(H_2)_2$ (top), $(D_2)_2$ (centre), and $(T_2)_2$ (bottom) dimers. For all three cases, we observe a small splitting effect between the two excited states.

model is a product of competing bound state vibrational shifts, which produces a higher overall vibrational shift compared to the originally more dominant $(1, 1, 2, 2, 0)$ state. Since the binding energy of the deuterium and tritium dimer ground states are larger in magnitude, we may not be able to neglect the anisotropic transitions in the Q region with the same success that we were able to obtain for the hydrogen dimer ortho-ortho and ortho-para Raman shifts. Furthermore, the actual nature of the binding states in terms of the four quantum numbers other than J is more complicated. While states were assigned using the dominant basis contributions to the resulting eigenfunctions, coupling cannot be completely neglected and varies between the ground and excited vibrational states. For instance, for para-para deuterium, this process of labeling quantum states seemingly leads to two nearly degenerate energy levels for the $(1, 1, 1, 2, 1)$ excited vibrational state. In practice, there appears to be significant coupling between this vibrationally symmetric $(1, 1, 1, 2, 1)$ state and the vibrationally antisymmetric $(1, 1, 2, 2, 1)$ state (both overall 'symmetric states' when rotational symmetry is also taken into account), hindering our ability to determine an accurate quantum state. For the calculations presented here, we consider both vibrational states as viable transitions for the $(1, 1, 1, 2, 1)$ ground state in accordance with the generally accepted method of labeling. Specifically, we assume that the intensity of each vibrational transition for this particular state is not diminished by the other (i.e. we include two $(1, 1, 1, 2, 1)$ ground state populations in our total dimer calculations). However, it is likely that these type of interactions would impose additional selection rules on the types of transitions that are permitted. Additional experimental work will be required to verify the observed shifts, in order to see if further refinement to this model is warranted.

3.3 IR spectroscopy

As a further means of assessing the success of this model in confirming spectroscopic results, we consider the Q(0) and Q(1) infrared shifts for the $(H_2)_2$ and $(D_2)_2$ dimers. Note that the vibrational states are above the thermal threshold for dissociation and are not stable as compared to the ground vibrational dimer states. However, the exact nature and population lifetimes of these states are not considered here in this section and remain a future area for research in both IR and Raman spectroscopy. McKellar[11] investigated separate spectra in this region for para-para hydrogen and ortho-ortho deuterium dimers, which were computed theoretically by Hinde.[19] However, the spectrum for normal hydrogen and deuterium dimers have not been explored. For this section, we provide a preliminary test of these results for ortho-ortho and ortho-para hydrogen pairs. In contrast to the previous section, we do not consider the relative intensity of each of these lines; unlike Raman spectroscopy, the peaks that occur for these lines are largely a result of induced dipole moments associated with the formation of dimers. There is also a weak quadrupole moment associated with the ortho H_2 monomer that is noted by McKellar on his spectra at a known position. Further analysis of these lines would require a more involved investigation of relevant dipole expansion terms, similar to work performed for rotational IR spectra.[12,53] For our current work, we only attempt to assign the known shifts provided in Table III for $(H_2)_2$ by McKellar,[11] using the selection rules $\Delta L_{end} = odd, \Delta J = 0, \pm 1$[58] as well as the additional restriction that $|\Delta L_{end}| \leq j_1 + j_2 + j_1' + j_2' + 1$.[59] Note that we do not attempt to assign quasibound ground states (i.e. $L_{end} > 1$ for $(H_2)_2$), $L_{end} > 3$ for $(D_2)_2$), which may explain the presence of a few additional

lines reported by McKellar, but not found in our calculations. We attempt to match our results as best as possible, using McKellar's Q(0) and Q(1) H_2 monomer spectral lines as baseline measurements for our shifts, to facilitate a more ready comparison. In general, our close-coupled approach yields accurate results, with these relatively simple selection rules. As seen with the Raman calculations, the primary purpose of these calculations is to help explore experimental work in this field using a well-defined PES. These results are presented in Table 3.6. The $(D_2)_2$ dimer produces a more complex vibrational IR spectrum. To help explore the accuracy of our potential for this isotolopologue, we first analyze the pure ortho deuterium dimers and produce identical results to those obtained previously by Hinde (Table 3.7). For these results, we are able to accurately assign a specific transition for each of the six spectral lines. For the normal deuterium spectrum, we do not attempt to accurately list all of the transitions since they are too numerous. Instead, we pick a single transition that is close to the reported experimental result where possible (Table 3.8), since these results are significantly more difficult to analyze as opposed to the pure ortho deuterium sample. Subsequent investigation into the strength of each transition will help elucidate which of the over 150 possible transitions dominate to produce this complex vibrational spectrum.

Table 3.6: Experimental and Calculated Q(0) and Q(1) IR $(H_2)_2$ Spectral Lines

Experimental Results[11] (cm^{-1})	Calculated Results (cm^{-1})	$(j_1'j_2'j_{12}'J'L_{end}') \leftarrow (j_1'j_2'j_{12}'JL_{end})$
4152.78(2)	—	—
4153.133(7)	4153.091	$(1,1,1,1,0) \leftarrow (1,1,1,0,1)$
	4153.140	$(1,1,2,2,0) \leftarrow (1,1,2,2,1)$
	4153.174^a	$(1,0,1,1,0) \leftarrow (1,0,1,1,1)$
4153.411(7)	4153.321	$(1,1,0,0,0) \leftarrow (1,1,0,1,1)$
	4153.406^a	$(1,0,1,1,0) \leftarrow (1,0,1,2,1)$
	4153.426	$(1,1,1,1,0) \leftarrow (1,1,1,2,1)$
	4153.456	$(1,1,2,2,0) \leftarrow (1,1,2,3,1)$
4153.67(2)	4153.644	$(1,1,1,1,0) \leftarrow (1,1,1,1,1)$
4153.76(2)	4153.744^a	$(1,0,1,1,0) \leftarrow (1,0,1,0,1)$
4153.96(2)	4153.955	$(1,1,2,2,0) \leftarrow (1,1,2,1,1)$
4155.61(3)	—	—
4156.04(3)	4156.006	$(1,1,2,1,1) \leftarrow (1,1,2,2,0)$
	4156.074^a	$(1,0,1,0,1) \leftarrow (1,0,1,1,0)$
4156.238(7)	—	—
4156.462(7)	4156.341	$(1,1,2,1,2) \leftarrow (1,1,2,2,1)$
	4156.399	$(1,1,1,1,1) \leftarrow (1,1,1,1,0)$
	4156.472^a	$(1,0,1,2,1) \leftarrow (1,0,1,1,0)$
	4156.559	$(1,1,2,3,1) \leftarrow (1,1,2,2,0)$
	4156.640	$(1,1,1,2,1) \leftarrow (1,1,1,1,0)$
	4156.733	$(1,1,0,1,1) \leftarrow (1,1,0,0,0)$
	4156.750^a	$(1,0,1,1,1) \leftarrow (1,0,1,1,0)$
4156.92(2)	4156.905	$(1,1,2,2,1) \leftarrow (1,1,2,2,0)$
4157.21(5)	4157.012	$(1,1,1,0,1) \leftarrow (1,1,1,1,0)$
	4157.156	$(1,1,2,1,2) \leftarrow (1,1,2,1,1)$
4158.03(5)	—	—
	4159.092^b	$(1,0,1,1,0) \leftarrow (1,0,1,1,1)$
	4159.324^b	$(1,0,1,1,0) \leftarrow (1,0,1,2,1)$
	4159.662^b	$(1,0,1,1,0) \leftarrow (1,0,1,0,1)$
	4162.001^b	$(1,0,1,0,1) \leftarrow (1,0,1,1,0)$
4162.41(3)	4162.393^b	$(1,0,1,2,1) \leftarrow (1,0,1,1,0)$
4162.51(2), 4162.513(5) (pure pH_2 sample)	4162.505	$(0,0,0,1,1) \leftarrow (0,0,0,0,0)$
4162.67(3)	4162.658^b	$(1,0,1,1,1) \leftarrow (1,0,1,1,0)$

^{a}Corresponds to excitation of ortho hydrogen in mixed pair

^{b}Corresponds to excitation of para hydrogen in mixed pair

Table 3.7: Experimental and Calculated Q(0) and Q(1) IR pure ortho $(D_2)_2$ Spectral Lines

Experimental Results[11] (cm^{-1})	Calculated Results (cm^{-1})	$(j_1'j_2'j_{12}'J'L_{end}') \leftarrow (j_1'j_2'j_{12}'JL_{end})$
2990.565(5)	2990.558	$(0,0,0,2,2) \leftarrow (0,0,0,3,3)$
2991.412(5)	2991.400	$(0,0,0,1,1) \leftarrow (0,0,0,2,2)$
2992.382(5)	2992.371	$(0,0,0,0,0) \leftarrow (0,0,0,1,1)$
2994.412(5)	2994.401	$(0,0,0,1,1) \leftarrow (0,0,0,0,0)$
2995.379(5)	2995.368	$(0,0,0,2,2) \leftarrow (0,0,0,1,1)$
2996.229(5)	2996.216	$(0,0,0,3,3) \leftarrow (0,0,0,2,2)$

Table 3.8: Experimental and Calculated Q(0) and Q(1) IR for normal $(D_2)_2$ Spectral Lines

Experimental Results[11](cm^{-1})	Calculated Results (cm^{-1})	$(j'_1j'_2j'_{12}J'L'_{end}) \leftarrow (j'_1j'_2j'_{12}JL_{end})$
2984.919(5)	—	—
2985.449(5)	2985.449^a	(1,0,1,1,0) ← (1,0,1,2,3)
2987.568(5)	2987.569^b	(1,0,1,1,0) ← (1,0,1,2,3)
2987.891(5)	2987.858	(1,1,1,2,2) ← (1,1,1,2,3)
2988.328(7)	2988.336^a	(1,0,1,3,2) ← (1,0,1,4,3)
2988.723(5)	2988.723^a	(1,0,1,0,1) ← (1,0,1,1,2)
2989.194(5)	2989.190^a	(1,0,1,2,1) ← (1,0,1,3,2)
2989.796(5)	2989.791^a	(1,0,1,1,1) ← (1,0,1,1,2)
2990.181(5)	2990.184^a	(1,0,1,1,0) ← (1,0,1,2,1)
2990.866(5)	2990.856^b	(1,0,1,0,1) ← (1,0,1,1,2)
2991.059(7)	2991.052	(1,1,2,2,0) ← (1,1,2,1,1)
2991.905(5)	2991.897^b	(1,0,1,1,1) ← (1,0,1,1,2)
2992.156(5)	2992.151^a	(1,0,1,2,1) ← (1,0,1,1,0)
2993.151(5)	2993.147^a	(1,0,1,3,2) ← (1,0,1,2,1)
2993.575(5)	2993.565^a	(1,0,1,1,2) ← (1,0,1,0,1)
2994.042(7)	2994.029^a	(1,0,1,3,3) ← (1,0,1,2,2)
2994.708(5)	2994.711^b	(1,0,1,1,2) ← (1,0,1,1,1)
2995.298(7)	2995.293^b	(1,0,1,2,2) ← (1,0,1,1,1)
2996.137(5)	2996.138^b	(1,0,1,4,3) ← (1,0,1,3,2)
2996.905(5)	2996.901^a	(1,0,1,2,3) ← (1,0,1,1,0)
2997.159(5)	—	—
2999.025(5)	2999.020^b	(1,0,1,2,3) ← (1,0,1,1,0)

^{a}Corresponds to excitation of para deuterium in mixed pair

^{b}Corresponds to excitation of ortho deuterium in mixed pair

3.4 Summary

We have used Hinde's 6D potential surface to calculate the bound states of spin isotopologues of dimers of molecular hydrogen. We have obtained the binding energy for the dimers, calculated with an exact diagonalization approach. Taking into account the additional complexity of these dimers, we have explored the Q(0) and Q(1) vibrational Raman shifts for each of these dimers using a simple Boltzmann weighted model, inclusive of total angular momentum degeneracy and symmetry considerations for each state. Our predictions are in line with the experimental measurements of Montero et al., with our inclusion of only isotropic scattering. We also provide predicted shifts for $(D_2)_2$ and $(T_2)_2$, in the hope that this will help provide further motivation for experimental studies with a higher resolution Raman vibrational spectrum. We have also provided some early success with the assessment of this potential for predicting and confirming IR vibrational dimer lines for hydrogen and deuterium dimers.

Chapter 4

Adiabatic Approach of Hydrogen Dimers

In this chapter, we extend the work discussed in Chapters 2 and 3 and outline specific details related to symmetry and basis choice. For instance, consider an alternative approach for computing binding state energies in which we separate the radial coordinate R from the other coordinates $(r_1, r_2, \theta_1, \theta_2, \phi_1, \phi_2)$. These included coordinates will also contain the dimer angles (θ_R, ϕ_R) as either full terms or parameters depending on whether the coordinate system is pinned. In cases where the grid or basis size is large, this adiabatic approach can prove to be quite valuable in reducing the computational cost of determining eigenvalues of the final energy matrix. Consider first a new form for the resulting Hamiltonian $(\hat{H}')$, where only the radial kinetic energy is removed from the adiabatic Hamiltonian $(\hat{H}_{adia})$:

$$\hat{H}' = -\frac{\hbar^2}{2\mu_{AB}R^2}\left(\frac{\partial}{\partial R}R^2\frac{\partial}{\partial R}\right) + \hat{H}_{adia} \tag{4.1}$$

Such that:

$$\hat{H}_{adia} = \hat{h}_1 + \hat{h}_2 + \hat{V}_{12} + \frac{1}{2\mu_{AB}R^2}\hat{L}^2_{end} \tag{4.2}$$

For a given value of R, the matrix elements $\langle \lambda | \hat{H}_{Adiabatic} | \lambda' \rangle$ can be determined. In particular, the smallest algebraic eigenvalue, or any eigenvalue of our choice, can be obtained for each value of R and labelled as $E_0(R)$. The kinetic energy operator can then be added back in to obtain the final matrix elements, before subsequent diagonalization of our new matrix:

$$\langle i | \hat{H}' | i' \rangle = \langle i | T_{rad} | i' \rangle + E_0(R_i)\delta_{i,i'} \tag{4.3}$$

The resulting binding energies suggest a number of important results, which are described in more depth below.

4.1 Primitive Basis Set

In this section, we provide a brief overview of the success of this simple approach for the three types of hydrogen dimer pairs, using the non-coupled basis set for para-para, ortho-para, and ortho-ortho hydrogen. All binding energies presented in this section were achieved with the same grid used in Chapter 3 (3.0 a_0 to 48.0 a_0, with intervals of 0.05 a_0) and a basis set where $j_{para,max} = 4$ and $j_{ortho,max} = 5$ unless otherwise stated.

4.1.1 Para-Para hydrogen

Over the course of these binding energy state calculations, the lowest eigenvalue (most negative in value) is taken at each radial point R and is assumed to represent the desired eigenvalue representing a consistent eigenstate. However, care must be taken to ensure that the basis is appropriately symmetrized. Due to the relative simplicity of para-para hydrogen,

our desired eigenstate consists largely of $j_1 = j_2 = 0$ character, with a single $m_1 = m_2 = 0$ non-degenerate state (i.e. the state is almost exclusively composed of $|0000\rangle$). Consequently, the lowest adiabatic curve is well-separated from other para-para hydrogen states that are composed of higher rotational character. However, symmetrization can still play an important role in the determination of the correct vibrational state. For the ground vibrational state, we obtain an adiabatic binding energy of -2.903 cm^{-1}. Notably, a failure to symmetrize the vibrational wavefunctions results in a change in the vibrational binding energy when the lowest adiabatic curve is picked, such that the calculated shift is -0.408 cm^{-1} instead of the obtained result of -0.406 cm^{-1}; in other words, the calculated vibrational binding energy varies from -3.311 cm^{-1} without symmetrization in comparison to a value of -3.309 cm^{-1} with symmetrization. This result occurs due to the crossing of the symmetric and antisymmetric vibrational states at low intermolecular distances; simply picking the lowest curve without symmetrization ensures that the antisymmetric vibrational state is sometimes selected instead. To illustrate this idea, the ground state vibrational para-para hydrogen dimer potential is presented in Figure 4.1, while the difference in energy between the symmetric and antisymmetric vibrational states is presented in Figure 4.2.

4.1.2 Ortho-Para hydrogen

The introduction of an ortho hydrogen molecule within a dimer pair leads to a new complexity, in comparison to a pure para-para hydrogen dimer. If we take a minimal basis $j_{ortho} = j_1 = 1$, $j_{para} = j_2 = 0$, we are left with three basis states $|j_1 m_1 j_2 m_2\rangle = |1000\rangle, |1\text{-}100\rangle, |1100\rangle$. For the full dimer, where end-over-end rotation is considered, the
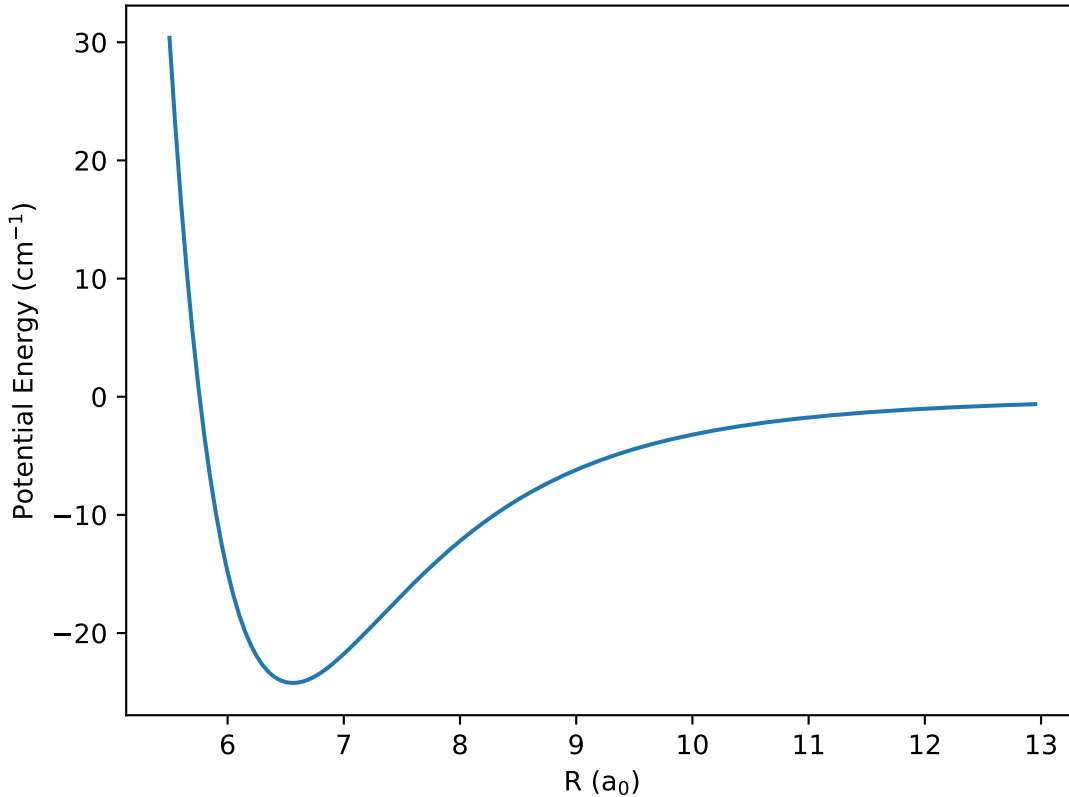
Figure 4.1: Potential energy, as a function of intermolecular distance R, for a ground rotational and vibrational state para-para hydrogen dimer.

state is independent of any m value and demonstrates three-fold degeneracy. However, when the dimer is fixed in space, a lower energy state is accompanied by a two-fold degeneracy. This idea is similar to previous work with endofullrenes, where an oH_2 molecule placed within a C_{60} structure also experienced identical symmetry breaking.[75,76] Similarly, an ortho hydrogen impurity within solid para hydrogen also produces a similar splitting pattern of a doubly degenerate and separate, single non-degenerate state.[5] For convenience, we often consider the dimer pair as situated along the z-axis. As described previously in Chapter 2, this configuration allows for a convenient setup such that the basis set is reduced based on
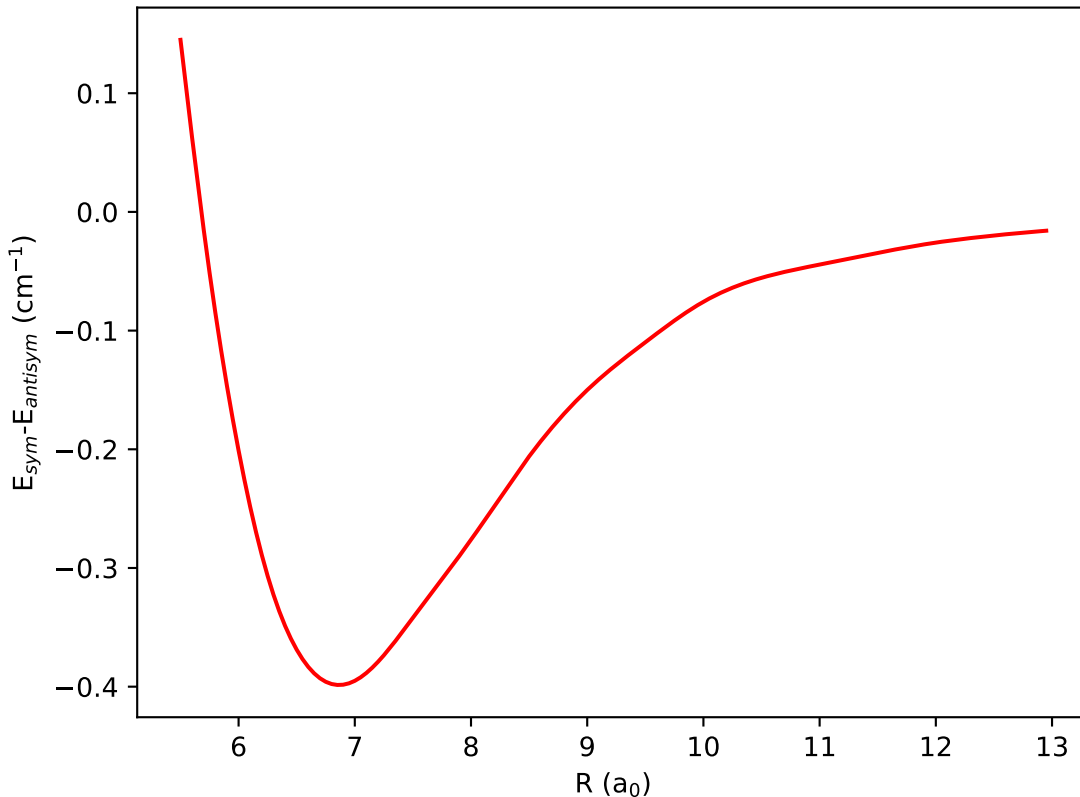
Figure 4.2: Difference in potential energy, as a function of intermolecular distance R, for symmetric and antisymmetric vibrationally excited, ground rotational state of the para-para hydrogen dimer.

the known definition for $Y_{l,m} = \delta m_0 \sqrt{\frac{2l+1}{4\pi}}$.[19] If we fix the dimer at a specific geometry, the energy eigenvalues are not affected. This idea is logical, since the rotation of the dimer in space only changes the relative molecular coordinate system. To consider this, recall that in a rotating dimer, the body fixed frame is typically set such that the z-axis lies along the collision coordinate, but it is equally valid to pick any other orientation for the collision coordinate.[39] In this case, we are simply defining a parameterized, fixed position of the dimer at the chosen coordinates, rather than allowing the dimer full rotation. As a result, the angles associated with each individual rotor spherical harmonic ((θ_i, ϕ_i) for each $Y_{j_i m_i}$)

still refer to the space fixed frame rather than a newly defined body fixed frame. In other words, we achieve 'similar' matrices, where the diagonalization of both matrices produces identical eigenvalues. However, as expected, there is a significant change in the character of the eigenvector (including complex terms in some cases). Consequently, it is much more convenient to employ a dimer fixed along the z-axis, where each eigenvector is dominated by a single basis state $|1m_100\rangle$. As shown in Chapter 2, we are also able to make use of decoupled basis states $m_1 + m_2 = m_1' + m_2' = n$, where n spans $\{-1, 1\}$. Specifically, we obtain degenerate binding energies dominated by $|1 \pm 100\rangle$ of -2.704 cm^{-1} and a non-degenerate, lower ground binding energy of -3.351 cm^{-1} dominated by the $|1000\rangle$ state. For the excitation of ortho hydrogen, we obtain corresponding vibrational binding energies of -2.990 cm^{-1} and -3.742 cm^{-1}, respectively. In Figure 4.3, we present a potential energy function for the ortho-para hydrogen dimer. Collectively, this results in an average Raman shift of about -0.321 cm^{-1}, which is a good match for the full diagonalization calculations, corresponding to the $(j_1, j_2, j_{12}, J, L_{end}) = (1, 0, 1, 1, 0)$ state. For the excitation of para hydrogen, we obtain similar vibrational binding energies of -2.995 cm^{-1} and -3.725 cm^{-1}, with an averaged shift of about -0.319 cm^{-1}.

4.1.3   Ortho-Ortho hydrogen

Ortho-ortho dimers present additional complexity to this adiabatic model by introducing further splitting, as discussed previously during our exploration of the theory of the potential energy matrix elements in Chapter 2. We can again determine relatively simple eigenvectors by imposing a fixed dimer location along the z-axis. Here, we obtain simple eigenstates
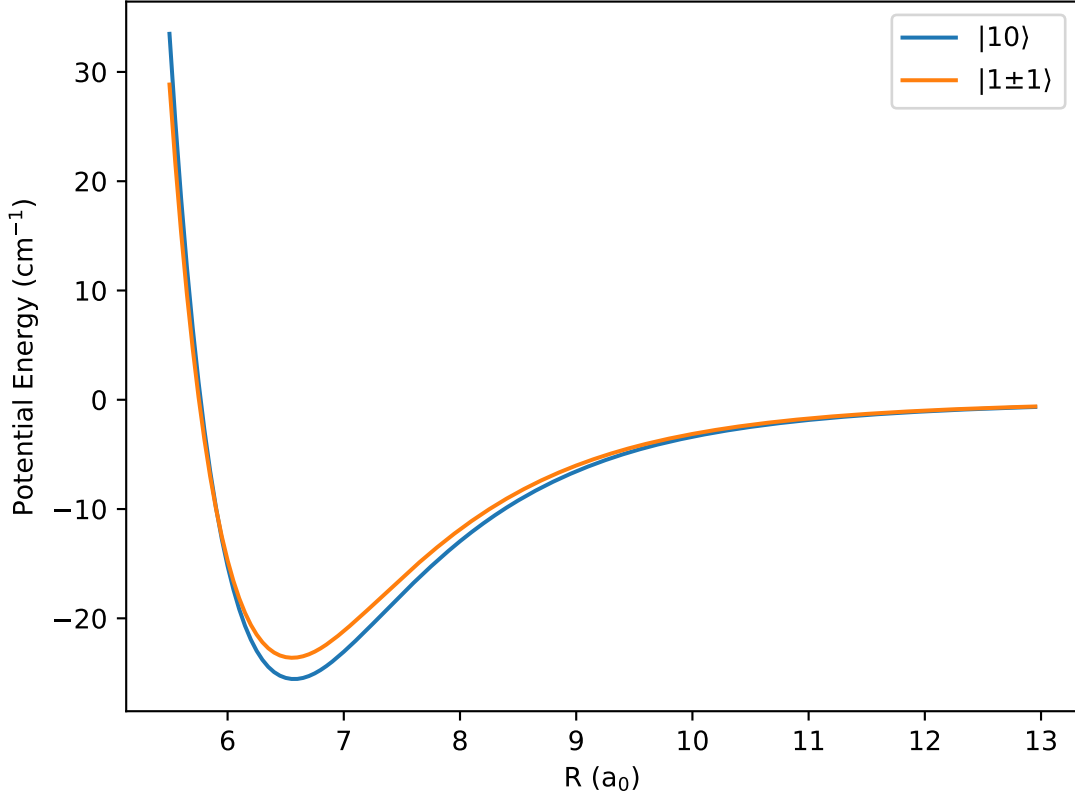
Figure 4.3: Potential energy, as a function of intermolecular distance R, for split energy levels of the ground rotational and vibrational states of the ortho-para hydrogen dimer.

that can be roughly approximated by the following expressions ($|m_1 m_2\rangle$), which loosely correspond to the equivalent coupled states given here:[5]

(1,2) $|m_1 m_2\rangle = |\pm 1 \pm 1\rangle$, $m_1 + m_2 = \pm 2$, $|j_{12}, m_{12}\rangle = |2, \pm 2\rangle$

(3,4) $|m_1 m_2\rangle = \frac{1}{\sqrt{2}}(|\pm 10\rangle + |0 \pm 1\rangle)$, $m_1 + m_2 = \pm 1$, $|j_{12}, m_{12}\rangle = |2, \pm 1\rangle$

(5,6) $|m_1 m_2\rangle = \pm \frac{1}{\sqrt{2}}(|\pm 10\rangle - |0 \pm 1\rangle)$, $m_1 + m_2 = \pm 1$, $|j_{12}, m_{12}\rangle = |1, \pm 1\rangle$

(7) $|m_1 m_2\rangle = \frac{1}{\sqrt{2}}(|\pm 1 \mp 1\rangle - |\mp 1 \pm 1\rangle)$, $m_1 + m_2 = 0$, $|j_{12}, m_{12}\rangle = |10\rangle$

(8) $|m_1 m_2\rangle = \frac{1}{\sqrt{6}}(|\pm 1 \mp 1\rangle + 2|00\rangle + |\mp 1 \pm 1\rangle)$, $m_1 + m_2 = 0$, $|j_{12}, m_{12}\rangle = |20\rangle$

(9) $|m_1 m_2\rangle = \frac{1}{\sqrt{3}}(|\pm 1 \mp 1\rangle - |00\rangle + |\mp 1 \pm 1\rangle)$, $m_1 + m_2 = 0$, $|j_{12}, m_{12}\rangle = |00\rangle$

Table 4.1: Binding Energies for Ortho-Ortho Hydrogen Dimer Adiabatic Model

Basis Set	$-E_{v=0}$ (cm^{-1})	$-E_{v=1}$ (cm^{-1})	$-\nu$ (cm^{-1})
(1,2)	2.170	2.443	0.274
(3,4)	4.716	5.418	0.702
(5,6)	3.132	3.577	0.445
(7)	2.497	2.820	0.323
(8)	1.188	1.331	0.142
(9)	3.265	3.742	0.477
Average	2.998	3.419	0.420

In the above states, $(1, 2), (3, 4)$, 8, and 9 are rotationally symmetric, while states $(5, 6)$ and 7 are rotationally antisymmetric. For the special $m_1 + m_2 = 0$ case, the lowest eigenvalues cannot be simply taken for each R value, as performed previously, since there is more than one possible eigenvalue corresponding to various ground rotational states. Similarly, for the vibrationally excited $m_1 + m_2 = \pm 1$, the rotationally symmetric (3,4) states can appear in an overall antisymmetric state, if it possesses antisymmetric vibrational delocalization. This can lead to errors in assignment due to energy curve crossings with the desired rotationally antisymmetric (5,6) states with a symmetric vibrational delocalization. Note that for the vibrational ground states, this is not a concern since there is no separate symmetric or antisymmetric vibrational states, meaning that the (3,4) and (5,6) states are generated separately using the symmetrization methods described in Chapter 2 purely on the basis of rotational symmetry. Instead, we can track the character of the eigenvalues at different R values to assign binding energies, such that we observe the following binding states (Table 4.1). This method ensures that the ground and vibrationally symmetric excited state share the same rotational eigenstate character. The final averaged value is relatively close to the approximate weighted averaged shift of the $(j_1, j_2, j_{12}, J, L_{end}) = (1, 1, 0, 0, 0), (1, 1, 2, 2, 0)$, and $(1, 1, 1, 1, 0)$ states. Drawing on these ideas, in Figure 4.4, we present a potential energy

function for the ortho-ortho hydrogen dimer. Notably, upon resolution of the resulting curves, we see that there is no crossing between the (8) and (9) curves, which have coupled eigenstates. The remaining curves are not exclusively non-crossing; however, as mentioned previously, curves with different $m_1 + m_2$ values do not interact. Furthermore, as was the case of vibrationally excited para-para hydrogen, states with either different rotational or vibrational symmetry appear to be decoupled from one another. For instance, there appears to be a crossing between the rotationally antisymmetric (5,6) and symmetric (9) states, which are treated separately in the symmetrized basis. If we refer back to the j_{12} states described in Chapter 2, we see that the generated states (1)-(9) are in relatively good agreement with the order of coupled states reported previously.

4.2   Additional Considerations for other basis sets

In the case of partial (j_{12}) and full (J) coupling, a similar problem can occur if the parity of the basis is not considered, which can introduce additional complications in assuming the lowest eigenvalue; here, the resulting adiabatic curve could be a mixture of non-coupling eigenstates if this idea is not taken into consideration. In addition, if a projection operator is used instead of a symmetrized angular wavefunction, there will be zero-value eigenvalues present after diagonalization. Consequently, at lower intermolecular distances, where the potential is positive, there could be artificial selection of eigenvalues of a so-called 'zero-energy curve' instead of the actual lowest adiabatic curve. As shown previously, an alternative method involves the selection of the eigenstates in terms of dominant eigenfunctions, instead of the simple lowest eigenvalue assumption. These results are more in line with the
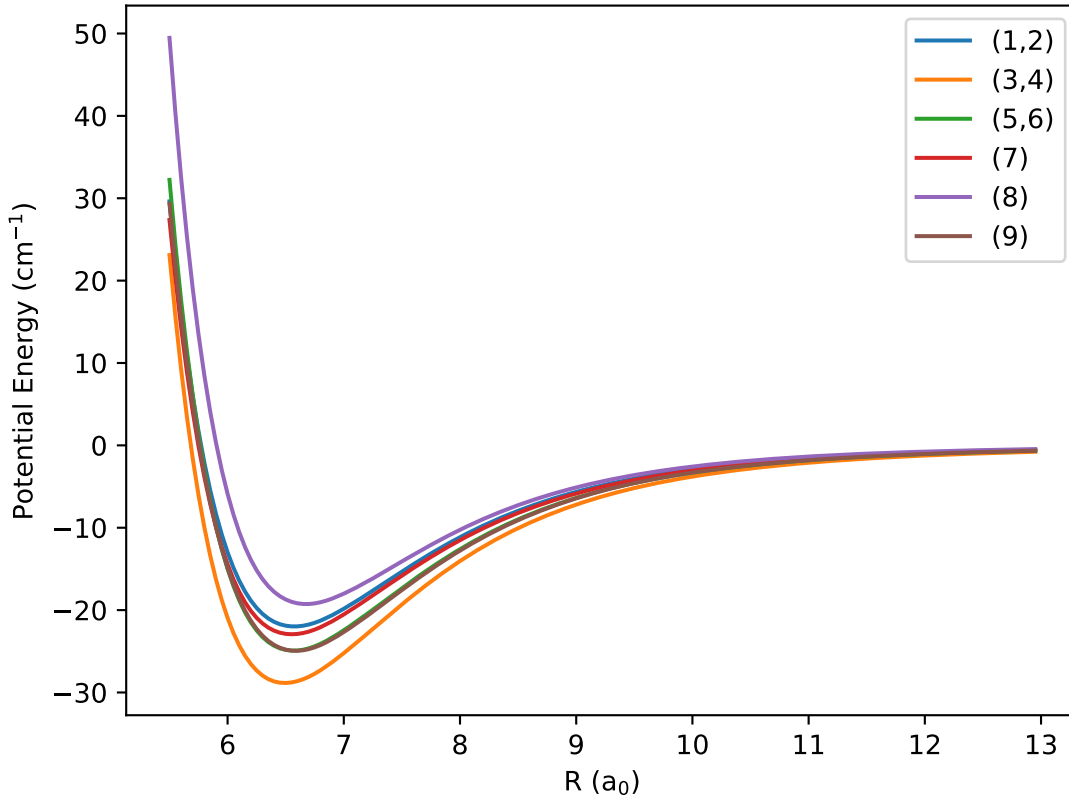
Figure 4.4: Potential energy, as a function of intermolecular distance R, for split energy levels of the ground rotational and vibrational states of the ortho-ortho hydrogen dimer.

approach taken in Chapter 3 during the full diagonalization description. These ideas present future opportunities for the exploration of the adiabatic model, beyond what is considered above for the ortho-ortho case. In particular, this problem is more challenging, since for the full diagonalization problem, we assumed that eigenvalues were dominated by a single eigenstate, rather than as a linear combination of states as used here for the primitive basis set. Consequently, we are no longer simply taking 'adiabatic states'; instead by looking for dominance of a single basis state over another, we introduce a situation in which adiabatic principles are no longer followed and curve crossing of coupled states is possible. Ongoing

research seeks to explore and compare the nature of these energy states.

Chapter 5

Hydrogen Chains

5.1 Overview of model

Drawing upon the work of the previous chapter, we now consider how we would approach creating a linear chain of hydrogen molecules that can be better exploited for future experimental designs. Previous research by Halverson et al.[77] focused on hydrogen fluoride molecules (interacting with a standard dipole-dipole potential) placed inside fullerene cages that are themselves housed within hollow carbon nanotubes. For our model, the more complex Hinde potential will be employed instead of the standard dipole-dipole interaction. In addition, for our hydrogen-based model, we do not include the cages, since the hydrogen potential would likely be negligible if shielding was applied (Figure 5.1). Consequently, we use our hydrogen-based system and the mathematical techniques described here as a template for a molecular design, where the actual strength of intermolecular forces will vary depending on the chosen system. The basis set employed in these calculations is the direct product of all of the individual rotor eigenstates and grows quickly as the number of rotors in the system is increased.[77] To best approach this problem, we consider the fact that each
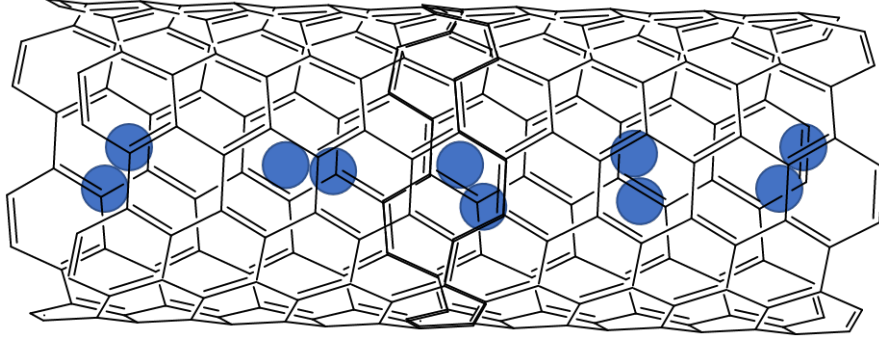
Figure 5.1: Model diagram of H_2, fixed in position in a carbon nanotube without C_{60} rings.

hydrogen molecule experiences $N - 1$ interactions, for a total of $\binom{N}{2} = \frac{N!}{2!(N-2)!}$ unique combinations. By generating a set of possible combinations using an efficient programming package (e.g. 'itertools' in Python), the appropriate radial matrix elements can be multiplied by the angular matrix elements. Note that the angular component of the hydrogen potential energy is not dependent on the distance between the rotors; this information can be calculated once and called as needed, as done previously in the dimer calculations. The resulting matrix elements for the combined potential matrix are simply the sum of each rotor pair's potential, with Kronecker delta functions added for any rotors that are not part of the specific interaction, i.e:

$$
\begin{aligned}
&\langle j_1 m_1 \nu_1 j_2 m_2 \nu_2 \ldots j_N m_N \nu_N | \, \hat{V} \, | j_1' m_1' \nu_1' j_2' m_2' \nu_2' \ldots j_N' m_N' \nu_N' \rangle \\
&= \sum_{a=2}^{N} \sum_{b=1}^{a-1} \langle j_a m_a \nu_a j_b m_b \nu_b | \, \hat{V}_{ab} \, | j_a' m_a' \nu_a' j_b' m_b' \nu_b' \rangle \prod_{c \neq a,b}^{N} \delta_{j_c j_c'} \delta_{m_c m_c'} \delta_{\nu_c \nu_c'}
\end{aligned}
\tag{5.1}
$$

For the purposes of this model, we assume that the dimers are fixed (i.e. $\hat{R} = (0,0)$). In other words, while each individual molecule can rotate freely, no end-over-end rotation can occur for the overall "dimers", with the overall motion of the rotors pinned. Consequently,

70

for every combination, the total energy of the system is described by the sum of the individual, diagonal Hamiltonian energies and the calculated potential from above. While current calculations will focus on ground state properties of the system (e.g. energy states), future work will also seek to explore various excited states. For instance, we hope to investigate a rotor containing a mix of ortho and para hydrogen molecules, with selective vibrational excitation of only some of the spin isomers. Since the overall size of the final matrix for any of these calculations can be quite large as N increases, two different methods can be employed in an effort to make the procedure more efficient.

5.1.1   Basis Truncation

As a means of reducing the size of the overall rotor matrix, several approaches to truncate the overall basis set are described by Halverson et al.[77] For instance, we can define some parameter limit J, such that for N rotors, the sum of all individual j_i is restricted by:

$$\sum_{i=1}^{N} j_i \leq J \tag{5.2}$$

As the value for J is increased, the calculated eigenvalues are expected to converge. As another method of basis truncation, Halverson et al. argue that the ground $|0\rangle$ state for the generic hydrogen fluoride system will have even parity for its total angular momentum (i.e. $\sum_{i=1}^{N} j_i = j_{tot}$, where j_{tot} mod $2 = 0$). In the case of pure para hydrogen, this is necessarily true; however, for pure ortho rotors or combinations of para and ortho hydrogen rotors, j_{tot} may be even or odd depending on the total number of each form of hydrogen and the length of the total chain. In any of the above cases, the total parity j_p is conserved, reducing the

size of the basis. A similar idea can be used to describe the sum of m_i, by assuming that each m_{tot} state forms a separate block; for our purposes, the $\sum_{i=1}^{N} m_i = m_{tot} = 0$ block is usually taken to be the lowest in energy and ideal for computing the ground state results. The final matrix is diagonalized as before using sparse matrix techniques; common methods rely on a FORTRAN library known as ARPACK that is often wrapped for use in C++ or Python using an Arnoldi method as described previously in Chapter 3.

5.2 Density Matrix Renormalization Group

When considering larger chains with as many as 50 rotors, Iouchtchenko and Roy[78] rely on a technique known as the density matrix renormalization group (DMRG) to allow for much more efficient computations. DMRG was first established by White[79] as an improvement over Wilson's[80] renormalization method in investigating magnetic impurities in metals. Typically used for one-dimensional systems (e.g. rotor chains), the conventional method for the finite-system version of DMRG is described by the following procedure:[79,81,82]

1. The chain or system is subdivided into a left block (S), a right block (E), and two sites in the middle. The combination of each of these parts forms a so-called "superblock" (length: $2L + 2$), with the S and E blocks both of length L.

2. The ground state ($|\psi\rangle$) of the superblock is computed using a variational approach and sparse diagonalization methods.

3. The reduced density matrix is calculated for each part of the system, i.e. $\hat{\rho}_E$, $\hat{\rho}_S$, and projected onto each block to form new states for S and E.

4. The E block gains an additional site from one of the two middle sites (new length: $L+1$).

To obtain a new middle site, the S block loses one additional site (new length: $L - 1$). Steps 2 and 3 are repeated, until the S block has a length of 0. The process is then repeated in the opposite direction, with the S block gaining a site and the E site losing a site during each iteration. When the two blocks reach equivalent length again, a "sweep" has occurred. To obtain an appropriately accurate ground state eigenfunction and energy eigenvalue, several sweeps may need to be performed.

During more recent investigations of DMRG, this procedure is usually thought of in terms of Matrix Product States (MPS). We divide the chain into two blocks A and B; using MPS, we note that the total Hilbert space of the chain ($\mathbb{H}$) is equal to the product of the two individual blocks' spaces (i.e. $\mathbb{H}_{\mathbb{A}} \otimes \mathbb{H}_{\mathbb{B}}$). The wavefunction of the entire system can be obtained using a mathematical procedure known as the Schmidt decomposition:[78]

$$|\Psi\rangle = \sum_i \sqrt{\lambda_i} \, |\phi_i^A\rangle \otimes |\phi_i^B\rangle \tag{5.3}$$

Where λ_i must be a non-negative, real number. We limit the total sum to some truncation parameter to prevent the exponential growth of the wavefunction. The reduced density matrices are calculated as before and projected onto blocks A and B, and repeated to complete sweeps. However, in order to exploit the block diagonal properties of these systems (related to $\sum_{i=1}^{N} j_i = j_{tot}$ and $\sum_{i=1}^{N} m_i = m_{tot}$ symmetry as discussed previously), the Hamiltonian must be written in terms of ladder operators that raise or lower j_i or m_i in a fixed manner.[78] For instance, for the dipole-dipole operator, the potential term along the z-axis was

expressed previously as:[78]

$$\hat{V}_{ij}^{(z)} = \hat{x}_i\hat{x}_j + \hat{y}_i\hat{y}_j - 2\hat{z}_i\hat{z}_j$$
$$= -2\hat{B}_i^0\hat{B}_j^0 + \frac{1}{2}[\hat{B}_i^-\hat{B}_j^+ + \text{h.c.}] \tag{5.4}$$

Where $\hat{B}_i^0 = \frac{1}{\hbar}(\hat{j}_i^+ + \hat{j}_i^-)$ and $\hat{B}_i^\pm = \pm\frac{1}{\hbar^2}\left([\hat{j}_i^+,\hat{m}_i^\pm] + [\hat{j}_i^-,\hat{m}_i^\pm]\right)$.

5.2.1 Exact Angular Potential Operators

For our hydrogen potential, we can use these ideas for the angular component of the operator, in which an analytical form is known. In particular, for the fixed dimer at $\hat{\boldsymbol{R}} = (0,0)$, we consider the operator $\hat{G}$, described previously in Chapter 2. Note that we use $\hat{\boldsymbol{r}}_i$ and $\hat{\boldsymbol{r}}_j$ for generic use in a multi-rotor model.

$$\hat{G} = \sqrt{\frac{2L+1}{4\pi}} \sum_m C_{l_1 m l_2 - m}^{L0} \hat{Y}_{l_1,m}(\hat{\boldsymbol{r}}_i)\hat{Y}_{l_2,-m}(\hat{\boldsymbol{r}}_j) \tag{5.5}$$

In addition, we rely on a table of spherical harmonics[6] to make the appropriate conversions between spherical harmonics and the one-body operators. Note the following relations:[78]

$$\hat{x}_i = \frac{1}{2\hbar^2}\left[(\hat{j}_i^+ + \hat{j}_i^-),(\hat{m}_i^+ - \hat{m}_i^-)\right] = sin\hat{\theta}cos\hat{\phi} \tag{5.6}$$

$$\hat{y}_i = \frac{1}{2i\hbar^2}\left[(\hat{j}_i^+ + \hat{j}_i^-),(\hat{m}_i^+ + \hat{m}_i^-)\right] = sin\hat{\theta}sin\hat{\phi} \tag{5.7}$$

$$\hat{z}_i = \frac{1}{\hbar}(\hat{j}_i^+ + \hat{j}_i^-) = cos\hat{\theta} \tag{5.8}$$

These definitions were used to define the operators $\hat{B}_i^0$ and $\hat{B}_i^{\pm}$, such that:

$$\hat{B}_i^{\pm} = \hat{x} \pm i\hat{y} \tag{5.9}$$

$$\hat{B}_i^0 = \hat{z}_i \tag{5.10}$$

Using this definition, the permitted expansions that result in non-zero terms are listed below for the analytical angular potential operator components in the space-fixed frame, where the rotors are fixed along the z-axis for convenience in deriving our equations. Here, we include a $(4\pi)^{-3/2}$ normalization factor for convenience, since we assume that the corresponding matrix element involving the $\hat{A}_{l_1,l_2,L}$ term takes into account this correction, as seen before.

$$\hat{G}_{000}(\hat{\boldsymbol{r_1}}, \hat{\boldsymbol{r_2}}, \hat{\boldsymbol{R}}) = \frac{1}{\sqrt{4\pi}} \frac{\hat{Y}_{0,0}(\hat{\boldsymbol{r_i}})\hat{Y}_{0,0}(\hat{\boldsymbol{r_j}})}{(4\pi)^{-3/2}} = \hat{1}_i \hat{1}_j \tag{5.11}$$

$$\hat{G}_{022}(\hat{\boldsymbol{r_1}}, \hat{\boldsymbol{r_2}}, \hat{\boldsymbol{R}}) = \sqrt{\frac{5}{4\pi}} \frac{\hat{Y}_{0,0}(\hat{\boldsymbol{r_i}})\hat{Y}_{2,0}(\hat{\boldsymbol{r_j}})}{(4\pi)^{-3/2}} = \hat{1}_i \frac{5}{2}(3\hat{B}_j^0 \hat{B}_j^0 - \hat{1}_j) \tag{5.12}$$

$$\hat{G}_{202}(\hat{\boldsymbol{r_1}}, \hat{\boldsymbol{r_2}}, \hat{\boldsymbol{R}}) = \sqrt{\frac{5}{4\pi}} \frac{\hat{Y}_{2,0}(\hat{\boldsymbol{r_i}})\hat{Y}_{0,0}(\hat{\boldsymbol{r_j}})}{(4\pi)^{-3/2}} = \frac{5}{2}(3\hat{B}_i^0 \hat{B}_i^0 - \hat{1}_i)\hat{1}_j \tag{5.13}$$

$$\hat{G}_{224}(\hat{\boldsymbol{r_1}}, \hat{\boldsymbol{r_2}}, \hat{\boldsymbol{R}}) = \sqrt{\frac{9}{4\pi}} \frac{1}{(4\pi)^{-3/2}} \Big[\hat{Y}_{2,-2}(\hat{\boldsymbol{r_i}})\hat{Y}_{2,2}(\hat{\boldsymbol{r_j}}) + \hat{Y}_{2,-1}(\hat{\boldsymbol{r_i}})\hat{Y}_{2,1}(\hat{\boldsymbol{r_j}})$$

$$+ \hat{Y}_{2,0}(\hat{\boldsymbol{r_i}})\hat{Y}_{2,0}(\hat{\boldsymbol{r_j}})$$

$$+ \hat{Y}_{2,1}(\hat{\boldsymbol{r_i}})\hat{Y}_{2,-1}(\hat{\boldsymbol{r_j}}) + \hat{Y}_{2,2}(\hat{\boldsymbol{r_i}})\hat{Y}_{2,-2}(\hat{\boldsymbol{r_j}}) \Big]$$

$$= 3 \Big[C_{2-222}^{40} \times \frac{15}{8} \hat{B}_i^- \hat{B}_i^- \hat{B}_j^+ \hat{B}_j^+ - C_{2-121}^{40} \times \frac{15}{2} \hat{B}_i^0 \hat{B}_i^- \hat{B}_j^0 \hat{B}_j^+$$

$$+ C_{2020}^{40} \times \frac{5}{4}(3\hat{B}_i^0 \hat{B}_i^0 - \hat{1}_i)(3\hat{B}_j^0 \hat{B}_j^0 - \hat{1}_j)$$

$$- C_{212-1}^{40} \times \frac{15}{2} \hat{B}_i^0 \hat{B}_i^+ \hat{B}_j^0 \hat{B}_j^- + C_{222-2}^{40} \times \frac{15}{8} \hat{B}_i^+ \hat{B}_i^+ \hat{B}_j^- \hat{B}_j^- \Big] \tag{5.14}$$

Where, the Clesbch-Gordan coefficients are exactly equal to:

$$C_{0000}^{00} = C_{2000}^{20} = C_{0020}^{20} = 1 \tag{5.15}$$

$$C_{2-222}^{40} = C_{222-2}^{40} = \frac{1}{\sqrt{70}} \tag{5.16}$$

$$C_{2-121}^{40} = C_{212-1}^{40} = 2\sqrt{\frac{2}{35}} \tag{5.17}$$

$$C_{2020}^{40} = 3\sqrt{\frac{2}{35}} \tag{5.18}$$

Each of the four angular expansions are in agreement with the properties of ortho and para hydrogen. Specifically, ortho hydrogen has odd j rotational states, while para hydrogen has corresponding even states. Based on the structure of each of the four terms, only raising and lowering operators of $\Delta j = 0, \pm 2$ are allowed. Consequently, this approach is in agreement with the matrix elements derived earlier for the exact diagonalization approach: odd and even j states for each molecule do not couple together and can be treated separately.

5.2.2   Singular Value Decomposition (SVD)

The operator method described above only works for a system in which we can describe the potential energy operator as a series of exact analytical operators. We can apply this for a fixed $A_{l_1,l_2,L}(R)$ value that does not depend on the value of j. In the case of our hydrogen potential energy operator, if we wish to consider multiple j_1 and j_2 values that contribute to the radial component of the potential energy, we must turn to an alternative approach as there is no analytical form for the $\hat{A}$ operator. Since the potential energy operator must be expressed in terms of one-body operators, we can decompose a potential

energy matrix V taken at a fixed R. To do this, we must first map this matrix from its usual configuration of $j_1 m_1 j_2 m_2$ by $j_1' m_1' j_2' m_2'$ to the new setup of $j_1 m_1 j_1' m_1'$ by $j_2 m_2 j_2' m_2'$ (n.b. for simplicity, we replace this notation with $n_1 = \{j_1 m_1\}$). We then perform a singular value decomposition, using an existing build-in-tool in Itensor, a software package available in C++ and Julia that can be used for performing DMRG-based calculations with a MPS approach.[83] Mathematically, the decomposition of this new matrix V_{map} can be represented by the following equation:

$$V_{map} = S\sigma T^{\dagger} \tag{5.19}$$

Where V_{map} is a rectangular matrix with dimensions a by b, S is a square matrix with dimensions a by a, σ is a diagonal, rectangular matrix with dimensions a by b and $T^{\dagger}$ is a square matrix with dimensions b by b. Our original matrix V is Hermitian. However, this is only true for V_{map} as well if the two rotors are identical (i.e. both para or ortho). In addition, S and $T^{\dagger}$ are not Hermitian (i.e. $S \neq S^{\dagger}$ and $T^{\dagger} \neq T$). The purpose of performing this method leads to a series of row and column vectors, which act as one-body operators for each rotor. In Itensor, the matrix multiplication is performed using an iterative sum. In practice, we see that the matrix multiplication can be truncated to a reduced γ value (where γ is less than the dimensions of both S and $T^{\dagger}$). Although the accuracy of the obtained energy values decreases with fewer terms, this factor can often be insignificant for potential energy matrices where many of the quantum states only exhibit weak coupling:

$$V_{map,n_1 n_1'}^{n_2 n_2'} = \sum_{\gamma} \sigma_{\gamma} S_{n_1 n_1', \gamma} T_{\gamma, n_2' n_2}^{\dagger} = \sum_{\gamma} \sigma_{\gamma} S_{n_1 n_1', \gamma} T_{n_2 n_2', \gamma} \tag{5.20}$$

$$n_1 n_2 \begin{bmatrix} & \\ & \end{bmatrix}^{n_1' n_2'} \rightarrow n_1 n_1' \begin{bmatrix} & \\ & \end{bmatrix}^{n_2 n_2'} = \begin{bmatrix} & \\ & \end{bmatrix} \times \begin{bmatrix} & \\ & \end{bmatrix} \times \begin{bmatrix} & \\ & \end{bmatrix}$$

$$n_1 n_1' \times n_1 n_1' \quad n_1 n_1' \times n_2 n_2' \quad n_2 n_2' \times n_2 n_2'$$

(a)

$$\approx \begin{bmatrix} & \\ & \end{bmatrix} \times \begin{bmatrix} & \\ & \end{bmatrix} \times \begin{bmatrix} & \\ & \end{bmatrix}$$

$$n_1 n_1' \times \gamma \quad \gamma \times \gamma \quad \gamma \times n_2 n_2'$$

(b)

Figure 5.2: Visual description of Singular Value Decomposition Process ($V_{map} = S\sigma T^{\dagger}$). For our matrix, the dimensional size of $n_1 n_1'$ are equal to $n_2 n_2'$ for identical rotors (i.e. both para or ortho). Note that **(a)** refers to the exact SVD method, while **(b)** refers to the truncated approach.

A visual description of this approach is presented in Figure 5.2. The true benefit of the SVD method is its overall ability to be applied to a broad range of systems. To exploit this approach, the user needs to provide one or more potential energy matrices, for a variety of intermolecular distances, to cover all significant pair interactions between rotors. Consequently, there is no need to determine individual analytical operators, which can often be a time consuming approach. Unfortunately, a necessary consequence of this method is limitations to the applicability of the block diagonal j_{tot} and m_{tot} symmetry; we require the full, non-symmetrized dimer matrix in order to construct the one-body rotors and cannot construct a reduced basis initially. However, we can apply an analytical and/or numerical cutoff as detailed in the next section to limit the memory requirements of the system.

5.3 Dipole-Dipole System

To assess the overall accuracy and functionality of the SVD approach, we begin with the simple case of the dipole system, previously described using an operator approach by Iouchtchenko and Roy.[78] Unlike the hydrogen-based system, the dipole operators are singular raising or lowering operators; consequently, both even and odd j values are valid for inclusion in our system. For simplicity, we construct our system along the z-axis using the potential energy operator described in Eq. 5.4. For a $l_{max} = 2$ system, we therefore have a total of 81 possible basis functions. Since we require a SVD of the full basis to obtain the one-site operators, we cannot exploit certain symmetries inherent in a system (see section 5.1.1). Preliminary investigations include a summation over all possible indices of the matrix and suggest a problem: the bond dimension (M) grows quickly as the summation increases, leading to memory errors in the resulting code. Fortunately, this seems to be a product of numerical precision errors; most of the singular values (σ_γ) are near zero $(< 10^{-15})$ and can be readily discarded without affecting the overall convergence of the system. Specifically, since the dipole operator is composed of a sum of three pairs of one-body operators, we can truncate the sum to three terms as well to obtain nearly identical results. We present a comparison of the energy values calculated using the methods described previously,[78] with our SVD-based approach (Figure 5.3). When we first introduce a matrix product operator (MPO) cutoff of 10^{-10}, our results begin to diverge at around N = 12, likely due to growing summation of errors. In general, for systems in which no analytical description is possible at all, the truncation value can be obtained by simply applying a fixed cut-off value for the singular
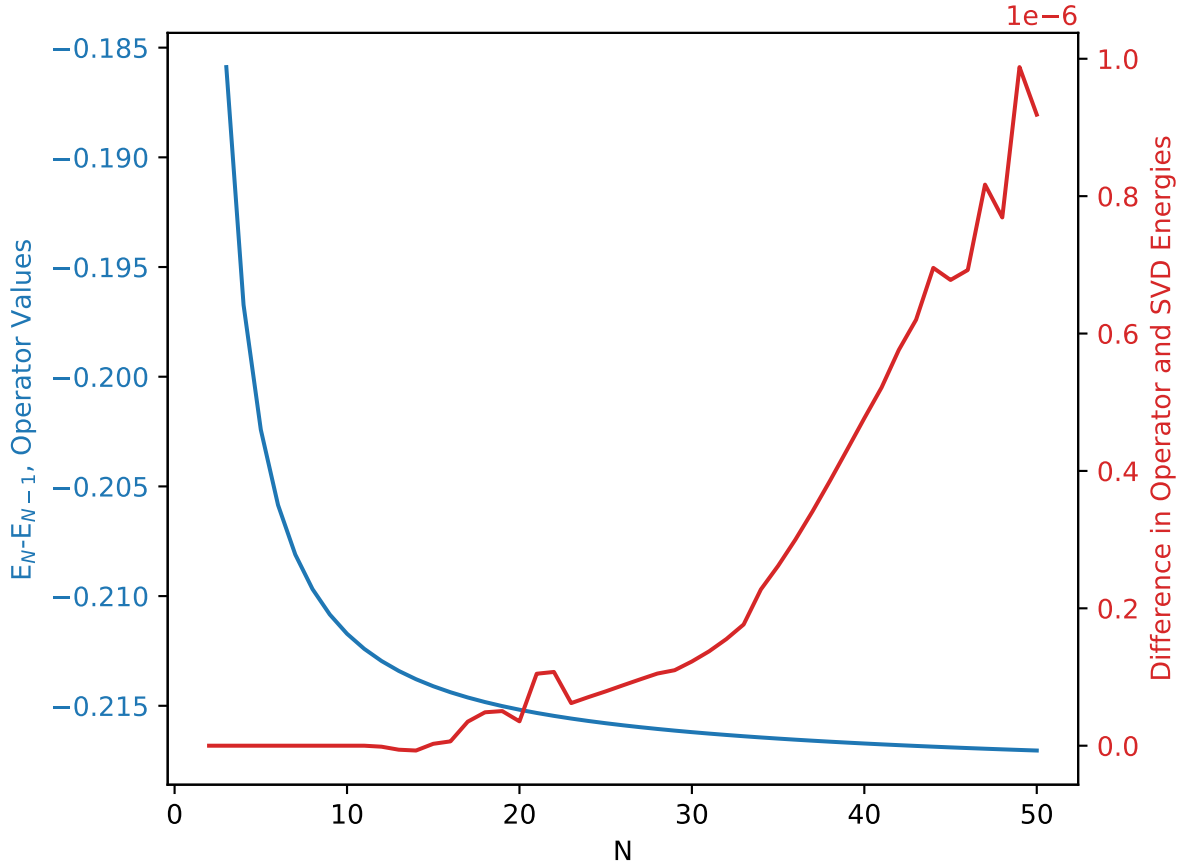
Figure 5.3: Comparison of results using the exact operator method described previously,[78] with SVD method proposed here for N = 2 to N = 50 rotors. Results are set for $j_{max} = 2$, with five DMRG "fast" sweeps and a MPO cutoff of 10^{-10}. Rotors are fixed apart at an arbitrary unit of $R = 1$.

values in the SVD. For instance, for our hydrogen-based system, we find that a cutoff of 12

terms produces appropriately converged results. Note that for all results presented in this

following hydrogen section, we assume a fixed intermolecular distance of 6.0 a_0.

Table 5.1: Ground state energy results (cm^{-1}) for pure para hydrogen rotors at varying J_{max} truncation, with $j_{max} = 4$. Note that the truncation value is given here in the form $^{J_{max}}E_0$.

N	$^{0}E_0$	$^{2}E_0$	$^{4}E_0$	$^{6}E_0$	$^{8}E_0$	$^{10}E_0$
2	-14.6816	-14.6821	-14.8407	-14.8407	-14.8407	-14.8407
3	-30.3758	-30.3773	-30.6949	-30.6949	-30.6949	-30.6949
4	-46.1524	-46.1551	-46.6316	-46.6316	-46.6318	-46.6318
5	-61.9433	-61.9472	-62.5826	-62.5827	-62.5830	-62.5830
6	-77.7379	-77.7431	-78.5373	-78.5373	-78.5379	-78.5379
7	-93.5338	-93.5402	-94.4931	-94.4932	-94.4941	-94.4941
8	-109.3301	-109.3377	-110.4493	-110.4494	-110.4507	-110.4507

5.4 Hydrogen-Based Chains

5.4.1 Para Hydrogen

Using the direct diagonalization method, we first include a table summarizing the ground state energy of pure para hydrogen chains, with varying maximum truncation values (J_{max}) (Table 5.1). We include all intermolecular potential pairs, for each of the interactions experienced for up to eight rotors. At this stage of development for our DMRG comparisons, we include two simplifications in comparison to the above results. We cap j_{max} at a value of 2 and only include the nearest neighbour calculations (i.e. in our DMRG code, this is referred to as a sociability value of 1). For comparison between exact diagonalization and DMRG, we present our results in Table 5.2 and find good agreement.

Table 5.2: Ground state energy results (cm^{-1}) for pure para hydrogen rotors at varying J_{max} truncation, with $j_{max} = 2$ and DMRG comparison, using our SVD approach. Note that the truncation value is given here in the form $^{J_{max}}E_0$.

N	$^0E_0$	$^2E_0$	$^4E_0$	$^6E_0$	$^8E_0$	$^{10}E_0$	$E_0^{DMRG,SVD}$
2	-14.6816	-14.6821	-14.8407	-14.8407	-14.8407	-14.8407	-14.8407
3	-29.3633	-29.3646	-29.6820	-29.6820	-29.6820	-29.6820	-29.6820
4	-44.0449	-44.0470	-44.5232	-44.5232	-44.5233	-44.5233	-44.5233
5	-58.7265	-58.7295	-59.3644	-59.3644	-59.3646	-59.3646	-59.3646
6	-73.4082	-73.4120	-74.2054	-74.2055	-74.2059	-74.2059	-74.2059
7	-88.0898	-88.0945	-89.0465	-89.0465	-89.0472	-89.0472	-89.0472
8	-102.7715	-102.7770	-103.8874	-103.8875	-103.8886	-103.8886	-103.8886

5.4.2   Ortho Hydrogen

In the case of pure ortho hydrogen chains, the more complicated nature of the molecule makes comparisons to our DMRG calculations more challenging. In particular, the employed software is able to find the lowest energy eigenvalues that is dominated by a single eigenstate (e.g. $|jm\rangle = |10\rangle$, $|1 \pm 1\rangle$). Consequently, while exact diagonalization is able to identify all relevant eigenenergies, including the lowest ground state, this property is not guaranteed for our DMRG approach. However, the eigenenergies still exhibit a final conserved $\sum m_i$ symmetry. In our DMRG code, if we set an initial test state of $|jm\rangle = |1 \pm 1\rangle$, our resulting energy corresponds to an orientation with all rotors having either $m_i = -1$ or $m_i = 1$ states (i.e. corresponding to a single eigenstate). If we instead set an initial test state of $|jm\rangle = |1 \pm 0\rangle$, we are left with a more complicated resulting ground eigenstate. The final eigenstates appear to be similar in form to the simple ortho-ortho eigenstate described previously in Chapter 4: $\frac{1}{\sqrt{3}}(|\pm 1 \mp 1\rangle - |00\rangle + |\mp 1 \pm 1\rangle)$ $(m_1 + m_2 = 0)$; however, the exact form becomes more complicated as the number of rotors increases. These findings suggest a current limitation for our DMRG approach. While para rotors exhibit a single low lying

energy state that is relatively easy to identify and determine, the introduction of multiple ortho hydrogen molecules results in a more difficult characterization, a factor that we have observed in our previous work on dimers that extends to the multi-rotor model. Ongoing work remains in helping to clarify and extend these results. It may also be worthwhile to consider a mixed system, where a chain of para hydrogen includes one or more ortho hydrogen 'impurities'.

Chapter 6

Conclusions

Ultimately, this thesis seeks to explore the physical and chemical nature of hydrogen-based systems, with extensions to various isotopologues. In particular, we have described a theoretical approach to the dimer system in line with a form for an exact, analytical potential derived previously. Using an accurate, *ab initio* potential developed by Hinde for the radial component of the potential, we have provided considerations for both full and adiabatic systems. We also include a basis for the calculations of chains, using both a full diagonalization approach and specific numerical tools involving DMRG (i.e. the operator approach and SVD).

Many of the techniques for determining the analytical potential energy matrix elements and symmetry relationships described in Chapters 2 and 3 were first developed over fifty years ago. However, as we have demonstrated, they are still applicable today and will likely continue to play a significant role for many years to come due to their continued importance in the investigation of van der Waals dimers. Future work in this field is divided into a number of different areas. As mentioned previously, improved spectroscopic measurements of dimers will allow for better fine-tuning and assessment of theoretical calculations; in

contrast to current measurements, new experimental data will likely have refined resolution that allows for the ability to more accurately assign Raman vibrational transitions similar to the work we describe at the end of Chapter 3 for IR vibrational transitions. There are also opportunities for future refinement for our theoretical model; for instance, the current monomer vibrational wavefunctions and energies are based on Le Roy's LEVEL code that relies on a baseline hydrogen monomer potential developed by Schwartz and Le Roy in 1987.[84] In addition, the "close-coupled channel" method used in this work is effective, but limited. In practice, the transitions described in the vibrational and IR spectrum cannot be fully described by a single eigenstate, as is conveniently employed in this thesis and throughout many papers within this field. For instance, as referred to previously in Chapter 3, the extent of coupling between various states that share four out of five quantum numbers likely plays some role in determining permitted and forbidden transitions.

6.1 Outlook and future directions

Although not explicitly described here, preliminary investigation has also looked at using updated potentials to describe trimer Raman vibrational shifts of $(H_2)_3$, $(D_2)_3$, and $(T_2)_3$. We achieve results in-line with experimental and theoretical findings first reported by Schmidt et al.;[23] however, in the case of trimers and large molecular clusters and materials (e.g. solid hydrogen[29]), three-body interactions are likely to play an important role in describing the overall potential.

In many respects, the processes reported throughout this thesis are designed for systems beyond $(H_2)_2$ and its isotopologues; investigation of related van der Waals dimers and chains

with larger intermolecular forces (e.g. $(N_2)_2$, $(O_2)_2$) may allow for additional considerations. In the case of chains, further investigation will look at binding between carbon nanotubes and various molecular units; this idea was neglected in Chapter 5 for simplicity when considering different representations of our pairwise sum of potential approach. The use of C_{60} or other rings to shield the intermolecular van der Waal or dipole forces may be required in the case of larger molecules, as outlined previously by Halverson et al.[77] The DMRG method described in this work also has broad applicability, with applications extending from the nearest neighbour approximation presented here. In particular, the SVD approach employed has the ability to incorporate any potential energy matrix beyond hydrogen (e.g. water based chains or systems). DMRG can also be applied beyond the simple 1D systems, into 2D or 3D configurations which may have greater practical applicability in the storage of hydrogen or other molecules.

References

[1] Kruger, P. *Int. J. Hydrog. Energy* **2000**, *25*, 1023–1033.

[2] Cherkasov, N.; Ibhadon, A. O.; Fitzpatrick, P. *Chem. Eng. Process* **2015**, *90*, 24–33.

[3] Cheng, H.-M.; Yang, Q.-H.; Liu, C. *Carbon* **2001**, *39*, 1447–1454.

[4] Struzhkin, V. V.; Militzer, B.; Mao, W. L.; Mao, H.-k.; Hemley, R. J. *Chem. Rev.* **2007**, *107*, 4133–4151.

[5] Van Kranendonk, J. *Solid Hydrogen: Theory of the Properties of Solid H_2, HD, and D_2*; Springer Science & Business Media: New York, 2012.

[6] Varshalovich, D.; Moskalev, A.; Khersonskii, V. *Quantum Theory Of Angular Momemtum*; World Scientific: Singapore, 1988.

[7] Hunter, J. D. *Comput. Sci. Eng.* **2007**, *9*, 90–95.

[8] Watanabe, A.; Welsh, H. L. *Phys. Rev. Lett.* **1964**, *13*, 810–812.

[9] McKellar, A. R. W.; Welsh, H. L. *Can. J. Phys.* **1974**, *52*, 1082–1089.

[10] McKellar, A. R. W. *Can. J. Phys.* **1984**, *62*, 760–763.

[11] McKellar, A. R. W. *J. Chem. Phys.* **1990**, *92*, 3261–3277.

[12] McKellar, A. R. W.; Schaefer, J. *J. Chem. Phys.* **1991**, *95*, 3081–3091.

[13] Schneider, B.; Hobza, P.; Zahradník, R. *Theor. Chem. Acc.* **1988**, *73*, 201–206.

[14] Senff, U. E.; Burton, P. C. *Aust. J. Phys.* **1989**, *42*, 47–58.

[15] Røeggen, I.; Wind, P. *Chem. Phys.* **1992**, *167*, 247–261.

[16] Diep, P.; Johnson, J. K. *J. Chem. Phys.* **2000**, *112*, 4465–4473.

[17] Kim, C. S.; Kim, S. J.; Lee, Y. S.; Kim, Y. H. *Bull. Korean Chem. Soc.* **2000**, *21*, 510–514.

[18] Patkowski, K.; Cencek, W.; Jankowski, P.; Szalewicz, K.; Mehl, J. B.; Garberoglio, G.; Harvey, A. H. *J. Chem. Phys.* **2008**, *129*, 094304.

[19] Hinde, R. J. *J. Chem. Phys.* **2008**, *128*, 154308.

[20] Schaefer, J. *Astron. Astrophys.* **1994**, *284*, 1015–1025.

[21] Tejeda, G.; Fernández, J. M.; Montero, S.; Blume, D.; Toennies, J. P. *Phys. Rev. Lett.* **2004**, *92*, 223401.

[22] Faruk, N.; Schmidt, M.; Li, H.; Le Roy, R. J.; Roy, P.-N. *J. Chem. Phys.* **2014**, *141*, 014310.

[23] Schmidt, M.; Fernández, J. M.; Faruk, N.; Nooijen, M.; Le Roy, R. J.; Morilla, J. H.; Tejeda, G.; Montero, S.; Roy, P.-N. *J. Phys. Chem. A* **2015**, *119*, 12551–12561.

[24] Li, H.; Roy, P.-N.; Le Roy, R. J. *J. Chem. Phys.* **2010**, *133*, 104305.

[25] Zeng, T.; Li, H.; Le Roy, R. J.; Roy, P.-N. *J. Chem. Phys.* **2011**, *135*, 094304.

[26] Wang, L.; Xie, D.; Le Roy, R. J.; Roy, P.-N. *J. Chem. Phys.* **2013**, *139*, 034312.

[27] Zhang, X.-L.; Ma, Y.-T.; Zhai, Y.; Li, H. *J. Chem. Phys.* **2018**, *148*, 124302.

[28] Diniz, L. G.; Mohallem, J. R. *J. Chem. Phys.* **2008**, *128*, 214306.

[29] Ibrahim, A.; Wang, L.; Halverson, T.; Le Roy, R. J.; Roy, P.-N. *J. Chem. Phys.* **2019**, *151*, 244501.

[30] Montero, S.; Morilla, J. H.; Tejeda, G.; Fernández, J. M. *Eur. Phys. J. D* **2009**, *52*, 31–34.

[31] Operetto, F.; Pederiva, F. *Phys. Rev. B* **2006**, *73*, 184124.

[32] Lide, D. R. *CRC Handbook of Chemistry and Physics, 85th edition*; CRC Press: Boca Raton, FL, 2005.

[33] Yoshioka, K.; Raston, P. L.; Anderson, D. T. *Int. Rev. Phys. Chem.* **2006**, *25*, 469–496.

[34] Oka, T. *Annu. Rev. Phys. Chem.* **1993**, *44*, 299–333.

[35] Hinde, R. J. *J. Chem. Phys.* **2003**, *119*, 6–9.

[36] Sears, V. F.; Van Kranendonk, J. *Can. J. Phys.* **1964**, *42*, 980–1003.

[37] Klar, H. *Z. Phys. A* **1969**, *228*, 59–67.

[38] Englot, G. F.; Rabitz, H. *Phys. Rev. A* **1974**, *10*, 2187–2205.

[39] Green, S. *J. Chem. Phys.* **1975**, *62*, 2271–2277.

[40] Schaefer, J.; Meyer, W. *J. Chem. Phys.* **1979**, *70*, 344–360.

[41] Brink, D. M.; Satchler, G. R. *Angular Momentum, 3rd edition*; Clarendon Press, 1993.

[42] Alexander, M. H.; DePristo, A. E. *J. Chem. Phys.* **1977**, *66*, 2166–2172.

[43] DePristo, A. E.; Alexander, M. H. *J. Chem. Phys.* **1977**, *66*, 1334–1342.

[44] Heil, T. G.; Green, S.; Kouri, D. J. *J. Chem. Phys.* **1978**, *68*, 2562–2583.

[45] Rabitz, H. *J. Chem. Phys.* **1972**, *57*, 1718–1725.

[46] Takayanagi, K. In *Advances in Atomic and Molecular Physics*; Bates, D. R., Estermann, I., Eds.; Academic Press, 1965; Vol. 1; pp 149–194.

[47] Wu, K.; Canning, A.; Simon, H. D.; Wang, L. W. *J. Comput. Phys.* **1999**, *154*, 156–173.

[48] Marr, A.; Halverson, T.; Tripp, A.; Roy, P.-N. *J. Phys. Chem. A* **2020**, *124*, 6877–6888.

[49] Le Roy, R. J. *J. Quant. Spectrosc. Radiat. Transf.* **2017**, *186*, 167–178.

[50] van der Avoird, A.; Wormer, P. E. S.; Moszynski, R. *Chem. Rev.* **1994**, *94*, 1931–1974.

[51] Burton, P. G.; Senff, U. E. *J. Chem. Phys.* **1982**, *76*, 6073–6087.

[52] Colbert, D. T.; Miller, W. H. *J. Chem. Phys.* **1992**, *96*, 1982–1991.

[53] Fletcher, L. N.; Gustafsson, M.; Orton, G. S. *Astrophys. J., Suppl. Ser.* **2018**, *235*, 24.

[54] Meurer, A. et al. *PeerJ Comput. Sci.* **2017**, *3*, e103.

[55] Wigner Symbols, SymPy (1.3), 2018, Available at https://docs.sympy.org/latest/modules/physics/wigner.html.

[56] ARPACK, Arnoldi Package, SciPy-ARPACK (1.2.0), 2018, Available at https://www.caam.rice.edu/software/ARPACK/, https://docs.scipy.org/doc/scipy/reference/tutorial/arpack.html.

[57] Simkó, I.; Szidarovszky, T.; Császár, A. G. *J. Chem. Theory Comput.* **2019**, *15*, 4156–4169.

[58] Bunker, P. R. *Can. J. Phys.* **1979**, *57*, 2099–2105.

[59] Bunker, P. R.; Jensen, P. *Molecular Symmetry and Spectroscopy, 2nd Ed.*; NRC Research Press: Ottawa, 1998.

[60] Khan, A.; Jahnke, T.; Zeller, S.; Trinter, F.; Schöffler, M.; Schmidt, L. P. H.; Dörner, R.; Kunitski, M. *J. Phys. Chem. Lett.* **2020**, *11*, 2457–2463.

[61] Anderson, L. W.; Pipkin, F. M.; Baird, J. C. *Phys. Rev.* **1960**, *120*, 1279–1289.

[62] Danby, G.; Flower, D. R. *J. Phys. B* **1983**, *16*, 3411–3422.

[63] Brocks, G.; van der Avoird, A. *Mol. Phys.* **1985**, *55*, 11–32.

[64] Danby, G. *J. Phys. B* **1989**, *22*, 1785–1807.

[65] Bounds, D. G. *Mol. Phys.* **1979**, *38*, 2099–2106.

[66] Li, X.; Ahuja, C.; Harrison, J. F.; Hunt, K. L. C. *J. Chem. Phys.* **2007**, *126*, 214302.

[67] Virtanen, P. et al. *Nat. Methods* **2020**, *17*, 261–272.

[68] Zucker, M., Kishore, A., Sukumar, R., Dragoset, R., Eds. *Elemental Data Index (version 2.5) [Online]*; 2017; Available at https://www.nist.gov/pml/

`elemental-data-index`, National Institute of Standards and Technol-ogy: Gaithers-burg, MD.

[69] Tiesinga, E., Mohr, P., Newell, D., Taylor, B., Eds. *"The 2018 CODATA Recommended Values of the Fundamental Physical Constants" (Web Version 8.1)*; 2019; National Institute of Standards and Technology, Gaithersburg, MD 20899, Available at `http://physics.nist.gov/constants`.

[70] Bernath, P. F. *Spectra of Atoms and Molecules*; Oxford University Press: New York, 2016.

[71] Niu, M. L.; Salumbides, E. J.; Dickenson, G. D.; Eikema, K. S. E.; Ubachs, W. *J. Mol. Spectrosc.* **2014**, *300*, 44–54.

[72] Lai, K.-F.; Hermann, V.; Trivikram, T. M.; Diouf, M.; Schlösser, M.; Ubachs, W.; Salumbides, E. J. *Phys. Chem. Chem. Phys.* **2020**, *22*, 8973–8987.

[73] Gustafsson, M.; Frommhold, L.; Bailly, D.; Bouanich, J.-P.; Brodbeck, C. *J. Chem. Phys.* **2003**, *119*, 12264–12270.

[74] Karman, T.; van der Avoird, A.; Groenenboom, G. C. *J. Chem. Phys.* **2015**, *142*, 084305.

[75] Kohama, Y.; Rachi, T.; Jing, J.; Li, Z.; Tang, J.; Kumashiro, R.; Izumisawa, S.; Kawaji, H.; Atake, T.; Sawa, H.; Murata, Y.; Komatsu, K.; Tanigaki, K. *Phys. Rev. Lett.* **2009**, *103*, 073001.

[76] Bačić, Z.; Vlček, V.; Neuhauser, D.; Felker, P. M. *Faraday Discuss.* **2018**, *212*, 547–567.

[77] Halverson, T.; Iouchtchenko, D.; Roy, P.-N. *J. Chem. Phys.* **2018**, *148*, 074112.

[78] Iouchtchenko, D.; Roy, P.-N. *J. Chem. Phys.* **2018**, *148*, 134115.

[79] White, S. R. *Phys. Rev. Lett* **1992**, *69*, 2863–2866.

[80] Wilson, K. G. *Rev. Mod. Phys.* **1975**, *47*, 773–840.

[81] Schollwöck, U. *Rev. Mod. Phys.* **2005**, *77*, 259–315.

[82] Schollwöck, U. *Ann. Phys.* **2011**, *326*, 96–192.

[83] Fishman, M.; White, S. R.; Stoudenmire, E. M. The ITensor Software Library for Tensor Network Calculations. 2020.

[84] Schwartz, C.; Le Roy, R. J. *J. Mol. Spectrosc.* **1987**, *121*, 420–439.

APPENDICES

Appendix A

Summary of Hydrogen and Deuterium Nuclear Spin Statistics

In Chapter 3, we make significant use of nuclear spin statistics as motivation for assigning symmetry, reducing the size of basis sets, and determining IR and Raman allowed transitions. Let us consider the nuclear spin statistics for $(H_2)_2$ and $(D_2)_2$, using the assigned symmetry of the wavefunctions and nuclear spin as described by Bunker.[58,58] Some important notes are included below:

1. We only assign symmetry states for ground rotational states since we are most interested in Q lines, without a change in rotational energy. In other words, we only include $|j_1 j_1 \pm\rangle$, where $j_1 = j_2$ for $j_1 = 0$ or $j_1 = 1$. Note that $|j_1 j_1 +\rangle$ is only allowed for even j_{12} and $|j_1 j_1 -\rangle$ is only permitted for odd j_{12}.

2. At equilibrium, the nuclear spin statistical weights are given as the following (note that symmetric or antisymmetric refers to the overall dimer wavefunction). We include the total I_T that can result from the addition of the two monomers:

$(H_2)_2$

para-para: $^1B_1^+$ (symmetric, $I_T = 0$)

ortho-para/para-ortho: $^3E^+$ ($I_T = 1$)

ortho-ortho: $^6A_1^+$ (symmetric, $I_T = 0, 2$), $^3B_2^+$ (antisymmetric, $I_T = 1$)

(D$_2$)$_2$

ortho-ortho: $^{21}A_1^+$, (symmetric, $I_T = 0, 0, 2, 2, 4$), $^{15}B_2^+$ (antisymmetric, $I_T = 1, 2, 3$)

para-ortho/ortho-para: $^{18}E^+$ ($I_T = 1, 1, 2, 3$)

para-para: $^6B_1^+$ (symmetric, $I_T = 0, 2$), $^3A_2^+$ (antisymmetric, $I_T = 1$)

3. The rovibrational weight, Γ_{rv}, is defined as $\Gamma_{rv} = |\nu_1\nu_2\pm\rangle |j_1j_2\pm\rangle |n\rangle |L_{end}\rangle$. The symmetries of each of these terms at various conditions is defined by Bunker in Table 3[58] and Table 16-2.[59] The product of this symmetry must satisfy the bosonic or fermionic nature of the components of each dimer pair and produces a corresponding statistical weight. Specifically, (H$_2$)$_2$ must have a final symmetry of either B_1^+ or A_1^- since individual hydrogen nuclei are fermions (antisymmetric upon exchange), while hydrogen molecules are bosons (symmetric upon exchange). In contrast, (D$_2$)$_2$ must have a final symmetry of A_1^+ or B_1^-, since both individual deuterium nuclei and molecules are bosons and must be symmetric upon exchange. The purpose of the section below is to provide assorted calculations for different possible scenarios that can arise when calculating the symmetry of Γ_{rv}, to determine whether or not its product with the corresponding nuclear spin produces an allowed or forbidden final state.

Para-Para Hydrogen, $|j_1j_2+\rangle$ only, since j_{12} is always even for $j_1 = j_2 = 0$

$|\nu_1\nu_2+\rangle$, $L_{end} = even$

$$\Gamma_{rv} = A_1^+ \otimes A_1^+ \otimes A_1^+ \otimes A_1^+ = A_1^+ \tag{A.1}$$

$$A_1^+ \otimes B_1^+ = B_1^+ (\text{symmetric n.s. (1)}) \tag{A.2}$$

$|\nu_1\nu_2-\rangle$, $L_{end} = even$

$$\Gamma_{rv} = B_2^+ \otimes A_1^+ \otimes A_1^+ \otimes A_1^+ = B_2^+ \tag{A.3}$$

$$B_2^+ \otimes B_1^+ = A_2^+ (\textbf{forbidden}) \tag{A.4}$$

$|\nu_1\nu_2+\rangle$, $L_{end} = odd$

$$\Gamma_{rv} = A_1^+ \otimes A_1^+ \otimes A_1^+ \otimes A_2^- = A_2^- \tag{A.5}$$

$$A_2^- \otimes B_1^+ = B_2^- (\textbf{forbidden}) \tag{A.6}$$

$|\nu_1\nu_2-\rangle$, $L_{end} = odd$

$$\Gamma_{rv} = B_2^+ \otimes A_1^+ \otimes A_1^+ \otimes A_2^- = B_1^- \tag{A.7}$$

$$B_1^- \otimes B_1^+ = A_1^- (\text{symmetric n.s. (1)}) \tag{A.8}$$

Ortho-Ortho Deuterium, $|j_1 j_2 +\rangle$ only, since j_{12} is always even for $j_1 = j_2 = 0$

$|\nu_1\nu_2+\rangle$, $L_{end} = even$

$$\Gamma_{rv} = A_1^+ \otimes A_1^+ \otimes A_1^+ \otimes A_1^+ = A_1^+ \tag{A.9}$$

$$A_1^+ \otimes A_1^+ = A_1^+ (\text{symmetric n.s. (21)}) \tag{A.10}$$

$|\nu_1\nu_2-\rangle$, $L_{end} = even$

$$\Gamma_{rv} = B_2^+ \otimes A_1^+ \otimes A_1^+ \otimes A_1^+ = B_2^+ \tag{A.11}$$

$$B_2^+ \otimes B_2^+ = A_1^+ (\text{antisymmetric n.s. (15)}) \tag{A.12}$$

$|\nu_1\nu_2+\rangle$, $L_{end} = odd$

$$\Gamma_{rv} = A_1^+ \otimes A_1^+ \otimes A_1^+ \otimes A_2^- = A_2^- \tag{A.13}$$

$$A_2^- \otimes B_2^+ = B_1^- (\text{antisymmetric n.s. (15)}) \tag{A.14}$$

$\left|\nu_1\nu_2-\right\rangle, L_{end} = odd$

$$\Gamma_{rv} = B_2^+ \otimes A_1^+ \otimes A_1^+ \otimes A_2^- = B_1^- \tag{A.15}$$

$$B_1^- \otimes A_1^+ = B_1^- \text{(symmetric n.s. (21))} \tag{A.16}$$

Ortho-Para/Para-Ortho Hydrogen and Ortho-Para/Para-Ortho Deuterium

$\left|\nu_1\nu_2+\right\rangle, L_{end} = even.$

$$\Gamma_{rv} = A_1^+ \otimes E^- \otimes A_1^+ \otimes A_1^+ = E^- \tag{A.17}$$

$$E^- \otimes E^+ = A_1^- (\text{ (Hydrogen, 3 n.s.)}, B_1^- \text{(Deuterium, 18 n.s.))} \tag{A.18}$$

$\left|\nu_1\nu_2+\right\rangle, L_{end} = odd.$

$$\Gamma_{rv} = A_1^+ \otimes E^- \otimes A_1^+ \otimes A_2^- = E^+ \tag{A.19}$$

$$E^+ \otimes E^+ = B_1^+ (\text{ (Hydrogen, 3 n.s.)}, A_1^+ \text{(Deuterium, 18 n.s.))} \tag{A.20}$$

Ortho-Ortho Hydrogen

$\left|j_1j_2+\right\rangle, \left|\nu_1\nu_2+\right\rangle, L_{end} = even.$

$$\Gamma_{rv} = A_1^+ \otimes B_1^+ \otimes A_1^+ \otimes A_1^+ = B_1^+ \tag{A.21}$$

$$B_1^+ \otimes A_1^+ = B_1^+ \text{(symmetric n.s. (6))} \tag{A.22}$$

$\left|j_1j_2-\right\rangle, \left|\nu_1\nu_2+\right\rangle, L_{end} = even.$

$$\Gamma_{rv} = A_1^+ \otimes A_2^+ \otimes A_1^+ \otimes A_1^+ = A_2^+ \tag{A.23}$$

$$A_2^+ \otimes B_2^+ = B_1^+ \text{(antisymmetric n.s. (3))} \tag{A.24}$$

$\left|j_1 j_2 +\right\rangle, \left|\nu_1 \nu_2 -\right\rangle, L_{end} = even.$

$$\Gamma_{rv} = B_2^+ \otimes B_1^+ \otimes A_1^+ \otimes A_1^+ = A_2^+ \tag{A.25}$$

$$A_2^+ \otimes B_2^+ = B_1^+ (\text{antisymmetric n.s. (3)}) \tag{A.26}$$

$\left|j_1 j_2 -\right\rangle, \left|\nu_1 \nu_2 -\right\rangle, L_{end} = even.$

$$\Gamma_{rv} = B_2^+ \otimes A_2^+ \otimes A_1^+ \otimes A_1^+ = B_1^+ \tag{A.27}$$

$$B_1^+ \otimes A_1^+ = B_1^+ (\text{symmetric n.s. (6)}) \tag{A.28}$$

$\left|j_1 j_2 +\right\rangle, \left|\nu_1 \nu_2 +\right\rangle, L_{end} = odd.$

$$\Gamma_{rv} = A_1^+ \otimes B_1^+ \otimes A_1^+ \otimes A_2^- = B_2^- \tag{A.29}$$

$$B_2^- \otimes B_2^+ = A_1^- (\text{antisymmetric n.s. (3)}) \tag{A.30}$$

$\left|j_1 j_2 -\right\rangle, \left|\nu_1 \nu_2 +\right\rangle, L_{end} = odd.$

$$\Gamma_{rv} = A_1^+ \otimes A_2^+ \otimes A_1^+ \otimes A_2^- = A_1^- \tag{A.31}$$

$$A_1^- \otimes A_1^+ = A_1^- (\text{symmetric n.s. (6)}) \tag{A.32}$$

$\left|j_1 j_2 +\right\rangle, \left|\nu_1 \nu_2 -\right\rangle, L_{end} = odd.$

$$\Gamma_{rv} = B_2^+ \otimes B_1^+ \otimes A_1^+ \otimes A_2^- = A_1^- \tag{A.33}$$

$$A_1^- \otimes A_1^+ = A_1^- (\text{symmetric n.s. (6)}) \tag{A.34}$$

$\left|j_1 j_2 -\right\rangle, \left|\nu_1 \nu_2 -\right\rangle, L_{end} = odd.$

$$\Gamma_{rv} = B_2^+ \otimes A_2^+ \otimes A_1^+ \otimes A_2^- = B_2^- \tag{A.35}$$

$$B_2^- \otimes B_2^+ = A_1^- (\text{antisymmetric n.s. (3)}) \tag{A.36}$$

The nuclear spin statistics are identical for para-para deuterium compared to the above results for ortho-ortho hydrogen, except that for our nuclear spin product, we multiply by B_1^+ instead of A_1^+ and A_2^+ instead of B_2^+ to give final allowed states as discussed previously.